

# Enhanced mitochondrial G-quadruplex formation impedes replication fork progression leading to mtDNA loss in human cells

Mara Doimo<sup>1,2,\*</sup>, Namrata Chaudhari<sup>1</sup>, Sanna Abrahamsson<sup>3</sup>, Valentin L'Hôte<sup>1</sup>, Tran V.H. Nguyen<sup>1</sup>, Andreas Berner<sup>1</sup>, Mama Ndi<sup>1</sup>, Alva Abrahamsson<sup>4</sup>, Rabindra Nath Das<sup>4</sup>, Koit Aasumets<sup>5</sup>, Steffi Goffart<sup>5</sup>, Jaakko L.O. Pohjoismäki<sup>5</sup>, Marcela Dávila López<sup>3</sup>, Erik Chorell<sup>4</sup> and Sjoerd Wanrooij<sup>1,\*</sup>

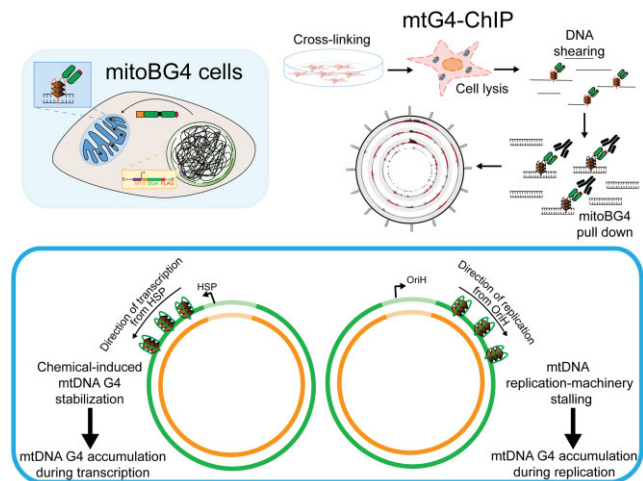
<sup>1</sup>Department of Medical Biochemistry and Biophysics, Umeå University, 90187 Umeå, Sweden, <sup>2</sup>Department of Women and Children Health, University of Padova, 35128 Padova, Italy, <sup>3</sup>Bioinformatics and Data Centre, Sahlgrenska Academy, University of Gothenburg, 41390 Gothenburg, Sweden, <sup>4</sup>Department of Chemistry, Umeå University, 90187 Umeå, Sweden and <sup>5</sup>Department of Environmental and Biological Sciences, University of Eastern Finland, FI-80101 Joensuu, Finland

Received June 08, 2022; Editorial Decision May 31, 2023; Accepted June 09, 2023

## ABSTRACT

Mitochondrial DNA (mtDNA) replication stalling is considered an initial step in the formation of mtDNA deletions that associate with genetic inherited disorders and aging. However, the molecular details of how stalled replication forks lead to mtDNA deletions accumulation are still unclear. Mitochondrial DNA deletion breakpoints preferentially occur at sequence motifs predicted to form G-quadruplexes (G4s), four-stranded nucleic acid structures that can fold in guanine-rich regions. Whether mtDNA G4s form *in vivo* and their potential implication for mtDNA instability is still under debate. In here, we developed new tools to map G4s in the mtDNA of living cells. We engineered a G4-binding protein targeted to the mitochondrial matrix of a human cell line and established the mtG4-ChIP method, enabling the determination of mtDNA G4s under different cellular conditions. Our results are indicative of transient mtDNA G4 formation in human cells. We demonstrate that mtDNA-specific replication stalling increases formation of G4s, particularly in the major arc. Moreover, elevated levels of G4 block the progression of the mtDNA replication fork and cause mtDNA loss. We conclude that stalling of the mtDNA replisome enhances mtDNA G4 occurrence, and that G4s not resolved in a timely manner can have a negative impact on mtDNA integrity.

## GRAPHICAL ABSTRACT



## INTRODUCTION

Mitochondria are key organelles as they are responsible for supplying the proper form of energy necessary for the cell to exert all its functions. Conversely to other cellular compartments, they possess their own circular, multi-copy DNA (mtDNA). The genes encoded by this small genome are essential for the function of the mitochondria (1). Qualitative (deletions) and/or quantitative (depletion) loss of the genetic information harboured in the mtDNA is detrimental to cellular homeostasis and, in humans, correlates with the onset of several pathological conditions collectively referred to as mtDNA maintenance defects (MDMD) (2).

\*To whom correspondence should be addressed. Tel: +46 722460309; Email: [sjoerd.wanrooij@umu.se](mailto:sjoerd.wanrooij@umu.se)  
Correspondence may also be addressed to Mara Doimo. Tel: +39 498216164; Email: [mara.doimo@unipd.it](mailto:mara.doimo@unipd.it)

One of the two strands of the mtDNA, the so-called 'heavy strand' (H-strand), is guanine-rich and harbours several sequences with the potential to form G-quadruplexes (G4s). G4s are non-canonical DNA secondary structures formed in nucleic acid sequences rich in guanines. In the human nuclear genome (nDNA), there are at least 700 000 sequences with the propensity to form G4s (3). G4s forming in nDNA are involved in the regulation of several cellular processes, such as replication, transcription and telomere maintenance (4). In mitochondria, G4s play a role in regulation of gene expression (5–7). In contrast, the *in vivo* distribution of G4s in the mtDNA and their implications in the process of mtDNA replication are still unknown. Nonetheless, *in silico* data show that putative G4-forming sequences (PGS) associate with pathogenic mtDNA deletion breakpoints (8,9).

However, the precise role of G4s in the process of mtDNA deletions formation has remained elusive, but work from the nDNA replication field has demonstrated that G4s may impede the progression of the nDNA replication machinery (10). Biochemical studies indicate that the formation of these structures might also interfere with mtDNA replication (9,11).

The study of G4s dynamics is limited due to the lack of tools to detect these structures in the cellular context. Recently, several groups developed synthetic antibodies or chemical compounds with fluorescent properties that specifically bind and recognize G4s. The first approach, employing synthetic antibodies, allows G4s detection in cultured cells using conventional immuno-techniques (12). Although G4s-specific antibodies proved to be useful to demonstrate the *in vivo* relevance of G4s, this method is subjected to specific manipulation (e.g. fixation and permeabilization) that can alter the G4 formation and eventually affect the antibody recognition (13). In addition, while this approach has been successfully employed to map G4 structures in the nuclear genome (14–16), it does not allow to specifically recognize G4s on the mtDNA without detecting nDNA G4s. In contrast, the second approach, employing chemical compounds, can be used in living cells, but often requires the use of non-conventional microscopy techniques (e.g. 2-photon microscopy (13) and FLIM (17,18)) and the compounds are generally strictly localized to the nucleus (19,20). Recently, fluorescent compounds were developed to monitor mtDNA G4s in living cells. However, these compounds do not permit to identify the specific localization of the G4s in the mtDNA (21–23).

To overcome these limitations, we established a cell model in which the G4-binding synthetic antibody BG4 (12) is specifically localized in the mitochondria and developed a chromatin immunoprecipitation approach to map specifically mtDNA G4s, called mtG4-ChIP. This method allowed us to map the regions in the mtDNA that accumulate G4s under physiological conditions. We then applied the mtG4-ChIP protocol to study the interplay between mtDNA G4s formation and the loss of mtDNA integrity.

## MATERIALS AND METHODS

### recBG4 purification

pSANG10-3F-BG4, for expression and purification of recombinant BG4 (BG4), was a gift from Shankar Balasub-

ramanian (Addgene plasmid # 55756). BG4 was purified as previously described (16).

### Cloning

The *MTSBG4* construct was synthesized by two-step overlap extension PCR. The *BG4* sequence was amplified by PCR from the pSANG10-3F-BG4 plasmid while the mitochondrial targeting sequence (MTS) of TFAM (aa 1–50) was amplified from the pcDNA5-FRT-TO-MTS-PRIMPOL construct (24). The reaction for the annealing PCR was performed with 0.5  $\mu$ L of a two-fold dilution of each reaction mixture from first-step amplifications. All amplifications were performed with Phusion polymerase (NEB) according to the manufacturer's instructions. The thermal conditions were as follows: 1 min at 98°C, followed by 20 cycles of 10 s at 98°C, 15 s at 55.8°C, and 30 s at 72°C, then 7 min at 72°C. The PCR product was then inserted into the pcDNA5-FRT-TO construct (ThermoFisher Scientific) using HindIII and EcoRV restriction sites following standard procedures. The oligonucleotides used for cloning are listed in Supplementary Table S5.

### Cell culture and compounds preparation

Flp-In T-Rex 293 (ThermoFisher Scientific) and U2OS (a gift from Luis Blanco, Centro de Biología Molecular Severo Ochoa, CSIC-UAM, Madrid, Spain) were maintained in DMEM high glucose + GlutaMAX (Life Technologies) supplemented with 10% fetal bovine serum (Sigma-Aldrich) and 1 mM pyruvate in standard incubation conditions at 37°C and 7% CO<sub>2</sub>. Upon integration of the MTS-BG4 gene, 50  $\mu$ g/ml uridine was added to the media. 2',3'-dideoxycytidine (ddC, Abcam) was freshly dissolved in distilled water to 100 mM prior to cell treatment. RHPS4 (TOCRIS) was dissolved to 10 mM in distilled water and stored at -20°C in small aliquots. PhenDC3 was purified as previously described (25), was dissolved to 50 mM in DMSO and stored at -20°C in small aliquots. Carbonyl Cyanide m-Chlorophenylhydrazone (CCCP, Sigma-Aldrich) was dissolved to 10 mM in DMSO and stored at -20°C.

### Generation of mitoBG4 cell lines ( $\rho^+$ and $\rho^0$ )

To express the mitochondrial targeted BG4 antibody in the cells, we took advantage of the Flp-In T-Rex system. We integrated the *MTS-BG4-FLAG* gene in the genome of the HEK (Human embryonic kidney) 293 Flp-In T-Rex (ThermoFisher Scientific).

This commercially available cell line contains a single integrated Flp Recombination Target (FRT) site at a transcriptionally active genomic locus and a TET repressor. It has been generated through the stable integration in the genome of HEK 293 cells of two plasmids: pFRT/lacZeo (which introduces the FRT site and the *lacZ*-Zeocin gene) and pcDNA6/TR (encoding the TET repressor and the Blasticidin resistance gene). The resulting cell line is Zeocin- and Blasticidin-resistant.

By co-transfection with the pOG44 plasmid (encoding a Flp recombinase) and pcDNA5/FRT/TO, which contains the *MTS-BG4-FLAG* gene under the control of

the CMV/TETO2 promoter and the Hygromycin resistance gene, the *MTS-BG4-FLAG* gene is integrated at the FRT position, upstream of the *lacZ-Zeocin* gene (leading to the disruption of its ORF). The resulting cell line is Hygromycin-resistant and Zeocin-sensitive.

Due to the presence of the TET repressor at the TETO2 site of the promoter, the expression of *MTS-BG4-FLAG* is inhibited in normal conditions. Upon addition of doxycycline, the TET repressor is displaced from the promoter and the gene of interest is transcribed.

The generation of the HEK 293 Flp-In T-Rex MTS-BG4 (mitoBG4) cell line was performed as previously described (26). Briefly, pcDNA5-FRT-TO MTS-BG4 was co-transfected with the pOG44 plasmid (ThermoFisher Scientific), in a 1:10 ratio, in an 80% confluent 10 cm plate using TurboFect Transfection Reagent (ThermoFisher Scientific). The day after transfection, cells were plated in five plates at differential dilutions and were cultured in the presence of 200  $\mu\text{g/ml}$  hygromycin B for several days until isolated colonies were visible. Hygromycin B resistant cells were pooled and kept in growth medium containing 100  $\mu\text{g/ml}$  hygromycin B. To allow the expression of MTS-BG4, doxycycline was added to the medium at the concentrations indicated for each experiment.

The mitoBG4  $\rho^0$  cell line was generated by keeping the cells in regular high glucose medium supplemented with 150 ng/ml Ethidium Bromide for 45 days. Depletion of mtDNA pools was measured at every cell passage by Multiplex PCR as described below. After complete depletion of mtDNA, cells were maintained on regular high glucose medium supplemented with pyruvate and uridine. Medium was changed every second day to avoid acidification. Before each experiment, cells were checked for complete depletion of mtDNA.

### Protein extraction and immunoblotting

Cells were lysed for 30 min on ice in RIPA buffer (150 mM NaCl, 1% NP-40, 0.1% SDS, 0.5% sodium deoxycholate, and 50 mM Tris-HCl (pH 8.0)). After high-speed centrifugation, the supernatant was collected for further analysis. Buffers for protein extraction were supplemented with 1 $\times$  EDTA-free Halt protease inhibitor cocktail (ThermoFisher Scientific). Protein amounts were quantified using a BCA protein assay kit (ThermoScientific). Equal amounts (15  $\mu\text{g}$ ) of proteins dissolved in 1 $\times$  Laemmli Sample Buffer (Bio-Rad) with 2.5%  $\beta$ -mercaptoethanol were separated on 4–20% SDS-TGX (Bio-Rad) gels and transferred to 0.45  $\mu\text{m}$  nitrocellulose membranes (GE Healthcare Life Sciences) using a Mini-Protean electrophoresis system (Bio-Rad). Membranes were blocked in 5% non-fat milk for 2 h. Primary antibodies were incubated overnight at 4°C, and horseradish peroxidase (HRP)-conjugated-secondary antibodies were incubated 1 h at room temperature. The antibodies used and their dilutions are listed in Supplementary Table S6. All washes and incubations were performed in Tris-buffered saline with Tween-20. Chemiluminescent detection was performed using ECL Western blot substrates (ThermoScientific) and a ChemiDoc Touch Imaging System (Bio-Rad).

For non-reducing SDS-PAGE, samples were extracted in NP-40 lysis buffer (150 mM NaCl, 1% NP-40, 10% gly-

cerol and 50 mM Tris-HCl (pH 8.0)) supplemented with 1X EDTA-free Halt protease inhibitor cocktail (ThermoFisher Scientific), 1 mM EGTA (pH 7.7), 5 mM ZnCl<sub>2</sub>, 5 mM NaF and 1 mM Na<sub>3</sub>VO<sub>4</sub>. Native samples were dissolved in non-reducing SDS Sample Buffer (10% SDS, 30% glycerol, 250 mM Tris-HCl (pH 6.8)) prior to SDS-PAGE separation and immunoblotting as described above. Recombinant BG4 (recBG4) was added as control.

### Cell fractionation and proteinase K accessibility assay

Cells were seeded in 15-cm plates in order to reach 80% confluency on the day of fractionation, and treated for 24 h with 10 ng/ml doxycycline. Cell fractionation and proteinase K accessibility assay were performed as previously described (24). Samples were analyzed by immunoblot as described above. Antibodies used are described in Supplementary Table S6.

### Immunofluorescence (IF) and co-localization analysis

IF was performed using a protocol modified from Jamroskovic *et al.* (27). Briefly, 60 000 cells were seeded on 13 mm glass coverslips the day before treatment. MitoBG4 cells were induced with 100 ng/ml doxycycline for 24 h. U2OS cells were treated with the indicated concentrations of CCCP or RHPS4 for 12 h. Cells were fixed in 2% paraformaldehyde for mitoBG4 cells or 4% formaldehyde for U2OS cells and permeabilized in 0.1% Triton X-100 at room temperature. Cells were blocked with 10% goat serum (mitoBG4 cells) or 2% BSA (U2OS) followed by incubation with antibodies diluted in 5% goat serum (mitoBG4 cells) or 0.1% BSA (U2OS). For primary antibodies, 0.1% TWEEN was added. Each incubation was performed for 1 h at 37°C in a humidified chamber. The antibodies used and their dilutions are described in Supplementary Table S6. All washes and incubations were performed in 1 $\times$  PBS buffer. Coverslips were mounted on glass slides with DAKO mounting medium (Agilent Technologies) and stored at 4°C.

Slides were imaged with Leica SP8 FALCON Confocal equipped with HC PL APO 63x/1.40 OIL CS2 objective. Fluorophores were excited sequentially with white light laser (WLL) and recorded with HyD detectors (Alexa Fluor 488: Ex: laser line 499, Em: 510–593 nm; Alexa Fluor 594: Ex: laser line 598, Em: 610–782 nm). Multiple z-stacks were collected for each field. A zoom of 3 was applied. Settings were optimized for co-localization analysis (28). Mander's correlation coefficient was measured with ImageJ (29) using the JaCoP plugin (28). Around 50 cells were analyzed for each experiment.

### Long term mitoBG4 expression

Cells were seeded in 6-well-plate at 200 000 cells/well and treatment with 10 ng/ml doxycycline was started the day after seeding. Cells were split 1:10 every third day and maintained in medium containing doxycycline. The remaining cells were used for immunoblotting and mtDNA copy number analysis as described in the respective sections.

### MtDNA copy number

MtDNA copy number was measured by multiplex PCR as previously described (30). Cells from the indicated treatment were collected by trypsinization and total genomic DNA was extracted using the PureLink Genomic DNA Minikit (ThermoFisher Scientific). Each DNA sample was diluted to 1 ng/ $\mu$ l and 2  $\mu$ l were used for amplification using PrimeTime Gene expression Master Mix (IDT) with Light-Cycler96 (Roche) instrument. Oligonucleotides for nuclear and mitochondrial DNA amplification and fluorescent labelled probes for signal detection are indicated in Supplementary Table S5. Each sample was run in triplicate. Mean Ct values were used to calculate the mtDNA copy number relative to untreated samples using the  $\Delta\Delta$ Ct method.

### Two-dimensional AGE (2D-AGE) and southern blotting

2D-AGE and subsequent Southern blot were performed as previously described (24). HincII (ThermoScientific) was used for mtDNA fragmentation. A PCR probe spanning nucleotides 35–611 (corresponding to the mtDNA non-coding region) random-prime labelled with [ $\alpha$ - $^{32}$ P]dCTP was used for nucleic acid hybridization.

For the analysis of sheared DNA samples for ChIP protocol, reverse cross-linked DNA was precipitated and purified using standard phenol-chloroform extraction. 2.5  $\mu$ g of non-sheared and sheared DNA was separated over a 1% agarose gel in 1 $\times$  TBE buffer. Southern blotting was performed by using standard procedures. An oligonucleotide mapping to the ND5 region of the mtDNA (Supplementary Table S5) was labelled at the 5'-end with [ $\gamma$ - $^{32}$ P]ATP using T4 Polynucleotide kinase (ThermoScientific) according to the manufacturer's instructions. Probe hybridization was performed using standard procedures (24). The membrane was exposed to a storage phosphor screen and scanned with the Typhoon Scanner 9400 (Amersham Biosciences).

### POLG DNA extension assay

The exonuclease-deficient catalytic subunit of polymerase  $\gamma$  POLG A and the processivity subunit POLG B were purified as previously described (31). The polymerase  $\gamma$  DNA extension assay was performed using a protocol modified from Jamroskovic *et al.* (27). Briefly, 20 nM of TET-labelled annealed template in reaction buffer (25 mM Tris-HCl (pH 7.6), 10 mM KCl, 25 mM MgCl<sub>2</sub>, 1 mM DTT, 100 ng/ $\mu$ l BSA, 200  $\mu$ M of dNTPs) was, when indicated, incubated with recBG4, PhenDC3 or RHPS4 at the specified concentrations at 37°C for 1 h. The reaction was then started by adding pre-incubated POLG A<sub>exo.</sub> and POLG B (62.5 nM and 93.75 nM respectively). The reactions were carried out at 37°C for 1, 5 or 20 min and blocked by the addition of 1:1 stop solution (95% formamide, 20 mM EDTA (pH 8) and 0.1% bromophenol blue). Denatured samples were separated over a 10% polyacrylamide Tris-borate-EDTA (TBE) gel containing 25% formamide and 8 M urea. The fluorescent signal was detected with a Typhoon scanner (Amersham Biosciences). The intensity of the full-length product and the G4 stalling band were quantified using Image Quant TL 10.2 software (GE Healthcare Life Sciences) and the ratio of full length to the G4 stalling band was calculated

and compared to the untreated reaction. Oligonucleotides used are listed in Supplementary Table S5.

### CD spectroscopy

3  $\mu$ M of each oligo were annealed/folded in 10 mM phosphate buffer (pH 7.4) with different KCl concentrations (as indicated in the figures legend) by heating for 5 min at 95°C and then overnight cooled to room temperature. A quartz cuvette with a path length of 10 mm was used for the measurements in JASCO-720 or JASCO-1700 spectrophotometers (Jasco International Co. Ltd). CD spectra were recorded at 25°C over  $\lambda = 195$ –400 nm with an interval of 0.2 nm, scan rate of 100 nm/min and 3 times accumulation. Oligonucleotides used are listed in Supplementary Table S5. CD melting curves for the pre-folded G4 DNAs were recorded at the maximum ellipticity wavelength between 20–95°C at a speed of 1°C/min.

### EMSA

1  $\mu$ M oligonucleotides was labelled at the 5'-end with  $\gamma$ - $^{32}$ P-ATP in a reaction catalysed by T4 polynucleotide kinase (PNK) for 60 min at 37°C. PNK was inactivated by incubating at 65°C for 10 min. Labelled oligonucleotides were purified on a G50 column (GE Healthcare). 100 nM of 5'- $^{32}$ P end-labelled G4 substrates in 1 mM Tris-HCl (pH 7.5) and 100 mM KCl were incubated at 95°C for 5 min and then allowed to cool down to room temperature to allow folding into G4 structures.

For the EMSA reaction, 1 nM folded G4 oligonucleotides (or scramble oligonucleotides) was mixed with increasing concentrations of BG4 (0, 1.56, 3.13, 6.25, 12.5, 25, 50 and 100 nM). Reactions (15  $\mu$ l) containing 1 mM Tris-HCl (pH 7.5), 0.25 mg/ml BSA, 0.1 M KCl, 10 nM MgCl<sub>2</sub> and 10% glycerol were incubated at 37°C for 10 min before separation over a 4.5% native acrylamide gel at 100 V for 35 min. Gels were dried for 1.5 h at 80°C before exposure to a storage phosphor screen. Bands were visualized using a Typhoon Scanner 9400 and ImageJ Software. Oligonucleotides used are listed in Supplementary Table S5. Recombinant MtSSB was purified as previously described (32).

### POLG and TWINKLE transient transfection

pCDNA3.1-POLG-MYC-HIS and pCDNA3.1-TWINKLE-MYC-HIS constructs were a gift from Hans Spelbrink (Radboud Center for Mitochondrial Medicine, The Netherlands). For each construct, 10 million cells/plate were plated in two 15 cm plates the day before transfection. 15  $\mu$ g of DNA was transfected with 45  $\mu$ l FuGENE HD transfection reagent (Promega) according to manufacturer's instructions. Cells were treated with 100 ng/ml doxycycline at the time of transfection. 24 h after transfection cells were processed for ChIP as described in the paragraph below.

### ChIP

For each treatment, 5 million cells/plate were plated in two 15 cm plates two days before harvesting (ca. 40 million

cells/plate were collected for each experiment). For  $\rho^0$  cells, four 15 cm plates were used (ca. 20 million cells/plate). Cells were treated with 100 ng/ml doxycycline for 24 h and, if needed, with 0.5  $\mu$ M of RHPS4 or 200  $\mu$ M ddC for 3 h.

Cross-linking was performed with 1% Methanol-Free Formaldehyde (Cell Signaling) in 1 $\times$  PBS for 10 min directly on the plates, followed by quenching with 125 mM glycine for 5 min. Cells were collected in ice-cold 1 $\times$  PBS, washed several times and lysed in 1 ml ChIP lysis buffer (140 mM NaCl, 50 mM HEPES–KOH (pH 7.5), 1 mM EDTA, 1% Triton X-100, 0.1% Sodium deoxycholate) supplemented with 1 $\times$  EDTA-free Halt protease inhibitor cocktail (ThermoFisher Scientific). DNA was sheared at 4°C for 1440 s with a Covaris E220 instrument to obtain mtDNA fragments of about 300–500 bp. Sonication conditions were as follows: duty cycle 5%, peak incident power 140.0 W, cycles per burst: 200. The sheared DNA was pre-cleared for 1 h with Pierce Protein A/G Magnetic Beads. 25  $\mu$ l and 10  $\mu$ l were collected at this stage as INPUT samples for immunoblot and sequencing analysis respectively. 350  $\mu$ l of each sample were then incubated overnight with 10  $\mu$ g of FLAG M2 antibody (Sigma) or mouse IgG (Santa Cruz) followed by 2 h and 30 min incubation with 20  $\mu$ l Pierce Protein A/G Magnetic Beads. Beads were collected using a magnetic rack and the supernatant was stored for protein analysis (non-bound fraction). Beads were subjected to subsequent washing steps with SDS Buffer (140 mM NaCl, 50 mM HEPES–KOH (pH 7.5), 1 mM EDTA, 0.025% SDS) two times, High salt wash buffer (1 M NaCl, 50 mM HEPES–KOH (pH 7.5), 1 mM EDTA), TL wash buffer (20 mM Tris–HCl (pH 7.5), 250 mM LiCl, 1 mM EDTA, 0.5% NP-40, 0.5% sodium deoxycholate), TE buffer two times. Samples were eluted in TE buffer with 1% SDS at 65°C for 2 min followed by vortexing. For sequencing and qPCR, samples were reverse cross-linked overnight at 65°C and treated with 100 ng/ml RNaseA for 15 min at 37°C and 20  $\mu$ g proteinase K for 2 h at 56°C to remove RNA and proteins respectively. The samples were finally purified with ChIP DNA clean and concentrator kit (Zymo Research). Samples were quantified by Qubit Fluorometer (ThermoFisher). ChIP-Seq library preparation and sequencing was performed by Novogen. Briefly, the DNA was subjected to mechanical fragmentation to achieve the proper size for library preparation. The NEBNext Ultra II DNA Library Prep Kit (New England Biolab) was used for sequencing library preparation according to the manufacturer's protocols. The library was quantified by Qubit Fluorometer (ThermoFisher) and real-time PCR, and size distribution was detected with Bioanalyzer (Agilent). Quantified libraries were pooled and sequenced on the Illumina NovaSeq 6000 sequencing platform. The sequencing strategy was pair-end 150 bp. Between 40M and 60M reads were generated for each individual sample.

For immunoblot analysis, samples were diluted in 1 $\times$  Laemmli Sample Buffer (Bio-Rad) with 2.5%  $\beta$ -mercaptoethanol and denatured before separation on SDS-PAGE as described above. For each sample, 10  $\mu$ l of immunoprecipitated fraction and 5  $\mu$ l of INPUT and unbound fraction were separated.

### ChIP-seq data analysis

The quality of the reads was examined using FastQC (0.11.2) (<https://www.bioinformatics.babraham.ac.uk/projects/fastqc/>).

A first analysis was performed using a standard pipeline for ChIP-Seq analysis from the Galaxy platform (33). Briefly, adaptors were removed with Trimmomatic (Galaxy Version 0.36.4), reads were mapped against Human genome hg38 using BWA-MEM (Galaxy Version 0.7.17.1) and non-uniquely mapped reads were removed using SAMtools Filter SAM or BAM (Galaxy Version 1.8+ galaxy) selecting a minimum MAPQ quality score of 20. Finally, peak calling for FLAG samples against IgG samples was performed using MACS2 (Galaxy Version 2.1.1.20160309.6). Unless otherwise stated, default parameters were applied in the analysis.

For manual peak calling, the reads were quality filtered using TrimGalore (0.4.0) ([https://www.bioinformatics.babraham.ac.uk/projects/trim\\_galore/](https://www.bioinformatics.babraham.ac.uk/projects/trim_galore/)) including reads with a minimum quality of 20 and a minimum length of 30. The Quality filtered reads were mapped towards the human reference genome (GRCh38) using BWA (0.7.5a) (34). To evaluate the quality of the ChIP-seq experiment, i.e. if there is significant clustering of enriched DNA sequence reads at locations bound by BG4, the cross-correlation of each sample was calculated using phantomPeaks (1.1) (35,36) yielding to NSC values between 1.005558 and 1.042857 and RSC values between 0.8999861 and 1.060696. PCR duplicates were removed using Picard (2.1.0) (<https://broadinstitute.github.io/picard/>) and artefacts in the genome (blacklist of GRCh38, ENCF356LFX) were removed using bamUtils (37) from NGSUtils (0.5.9-b4caac3) (38). Enrichment plots were generated with deepTools (2.5.1–1-e071ca1) (39) to assess if the antibody-treatment was sufficiently enriched to separate the ChIP signal from the background signal.

The depth per position and the total amount of high-quality mapped reads (Q20) towards the mitochondria (MT) was calculated using SAMtools (1.9) (40). Only positions with depth higher than 50 were included in further analyses. The samples were normalized for sequencing depth by dividing each position with the total number of mapped reads in the MT for each sample and multiplied by 100. The ratio between the FLAG sample and the INPUT sample was calculated adding a pseudo-count of 1. An in-house script was used to identify the resulting peaks. Positions with at least 50 contiguous nucleotides with a ratio of at least one were selected. The resulting range is reported as the broad peak. From the summit (highest ratio within the peak)  $\pm$ 50 bp were extracted as narrow peak coordinates. Finally, to visualize the peaks coverage, circular plots were generated using Circos (0.69) (41). The linear plots displaying the averages of the sample ratios were generated in R (4.0.1) (<https://www.r-project.org/>).

### qPCR

2  $\mu$ l of FLAG or IgG pull down and of a 1:10 dilution of the INPUT was used for amplification using qPCR-

BIO SyGreen Mix (PCR Biosystem) in a LightCycler96 (Roche) instrument. Oligonucleotides for nuclear and mitochondrial DNA amplification are indicated in Supplementary Table S5. Each sample was run in triplicate. Mean Ct values were used to calculate the amount of FLAG and IgG signal with respect to the INPUT. Mean Ct values of the INPUT were corrected for the dilution factor.

## ELISA

ELISAs were performed as previously described (42). 5  $\mu$ M of biotinylated oligos (Supplementary Table S5) were annealed in the Folding buffer (FB) (10 mM Tris-HCl, pH 7.4, 100 mM KCl) by heating (5 min 95°C) followed by overnight cooling to 25°C. Annealed oligos (Supplementary Figure S7 concentrations are indicated in the figure legend) were immobilized on Streptavidin High Binding Capacity Coated 8 well strips (Pierce). Where indicated, immobilized oligos were incubated with 250 nM G4 ligands in FB. Subsequently, RecBG4 in FB buffer (see Supplementary Figure S7 for concentrations) was added and incubated for 1 h with gentle shaking. After washing with ELISA Wash Buffer (EWB: 100 mM KCl + 50 mM KH<sub>2</sub>PO<sub>4</sub>) to remove unbound recBG4, strips were blocked using Blocking buffer (BB: 3% BSA in EWB) and subsequently incubated with mouse anti-FLAG antibody (1/5000 dilution in BB) and anti-mouse HRP antibody (1/10 000 dilution in BB) (1h with with gentle shaking). Several washes with EWB with TWEEN 0.1% were applied. Incubation steps were in 50  $\mu$ l volume/well and washes were performed in 200  $\mu$ l volume/well.

The HRP signal was detected using TMB ELISA Substrates (Pierce) according to manufacturer's instruction. The reaction was stopped with 2N HCl and the signal intensity was measured at 450 nm on a FLUOstar microplate reader (BMG Labtech).

## Statistical analysis

Samples size and number of replicates are indicated for each experiment. Two tail two samples *t*-test with assumed equal variance was used to determine significant differences. Variance was determined by *F* test. A *p*-value <0.05 was considered significant. All calculations were performed in Microsoft Excel and Origin 2017 software.

## RESULTS

### Establishing a cell line expressing mitochondrial targeted BG4 (mitoBG4)

To detect the formation of G4s specifically in the mtDNA in human cell lines without interfering with the G4s in the nucleus, we took advantage of the BG4 antibody. BG4 is a single chain antibody fragment that can specifically recognize G4s and was previously used to analyze nDNA and RNA G4s in fixed cells (12). We established a cell line expressing a variant of BG4 (mitoBG4) that is targeted to the matrix of mitochondria, where the mtDNA resides. To ensure the correct mitochondrial localization, the BG4 sequence with C-terminal FLAG tag was fused to the mitochondrial targeting signal (MTS) of TFAM (mitochondrial transcription

factor A) (24). The obtained *MTS-BG4-FLAG* sequence was subsequently inserted in the genome of HEK 293 cells using the Flp-In T-Rex system (see the method section 'Generation of the mitoBG4 cell lines' for more details). This system permits the locus-specific integration of the gene of interest under the control of a doxycycline-inducible promoter, thus allowing the modulation of gene expression (Supplementary Figure S1A). Upon induction with doxycycline, the integrated *MTS-BG4-FLAG* gene is transcribed and translated in the cell cytoplasm. MTS-BG4-FLAG is driven into the mitochondrial matrix due to the presence of the MTS. Once there, the MTS is recognized by specific proteases and removed, resulting in mitoBG4, a mitochondrial localized BG4 nearly identical to the recombinant BG4 (Supplementary Figure S1B).

Upon induction with doxycycline, the expression of mitoBG4 was detected by Western blot using an antibody against the FLAG tag. We detected a time- and dose-dependent expression of mitoBG4 (Supplementary Figure S1C). Two bands were visible, a higher molecular weight band corresponding to mitoBG4 retaining the MTS peptide and a lower band corresponding to mitochondrially imported mitoBG4 with cleaved MTS. The same band pattern is present in TFAM-overexpressing cells (43).

### mitoBG4 localizes to mitochondria and is properly folded

We then looked at the localization and folding of mitoBG4 within the cellular environment. Immunofluorescence (IF) with the mitochondrial marker TOM20 revealed co-localization of mitoBG4 with mitochondria (Figure 1A and B), which was further confirmed by a fractionation assay (Supplementary Figure S1D). In addition, a Proteinase K accessibility (PKA) assay demonstrated that mitoBG4 was localized to the mitochondrial matrix, similar to the mitochondrial single stranded DNA-binding (mtSSB) protein, as it was protected against Proteinase K digestion unless the inner mitochondrial membrane was solubilized (Figure 1C).

Finally, since BG4 corresponds to the fragment crystallisable region (scFv fragment) of the antibody and requires formation of disulfide bonds to be properly folded, we performed non-reducing SDS-PAGE to test its intracellular conformation. Separation of protein extracts from induced mitoBG4 cells in non-reducing conditions revealed that native mitoBG4, like the recombinant BG4 (recBG4), run at different size than its reduced counterpart (treated with  $\beta$ -mercaptoethanol), suggesting that mitoBG4 protein forms disulphide bonds when expressed in the cells (Figure 1D).

Taken together, these data indicate that mitoBG4 localizes and properly folds in the mitochondrial matrix, where the mtDNA also resides.

### mitoBG4 co-localizes with mitochondrial nucleoids

We then set out to analyse whether mitoBG4 interacts with the mitochondrial nucleoids, the nucleoprotein complexes in which the mtDNA is organized. IF of induced mitoBG4 cells showed that mitoBG4 protein co-localizes with TFAM, the main mtDNA nucleoid component (Figure 2A and C). This co-localization was comparable to that of mi-

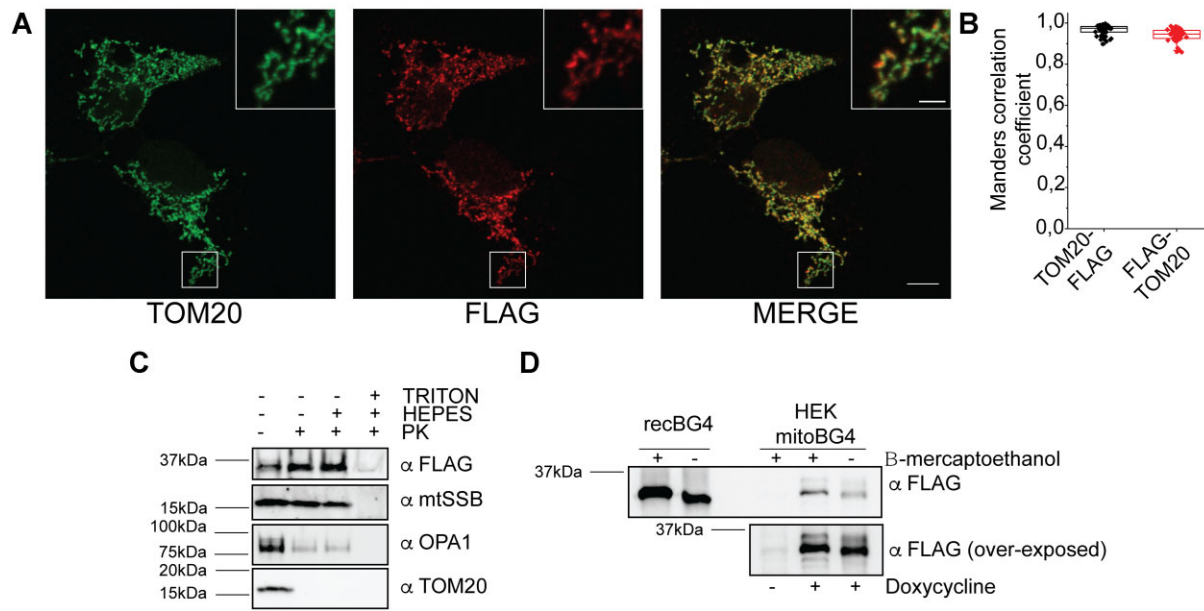


**Figure 1.** mitoBG4 is localized in the mitochondrial matrix and is properly folded. (A) Representative immunofluorescence images of induced mitoBG4 cells immunolabeled with FLAG antibody (to detect mitoBG4) and TOM20 (mitochondrial outer membrane marker) antibody. Scale bars: 10  $\mu\text{m}$  and 2  $\mu\text{m}$  in the magnified box. (B) Quantification of the reciprocal co-localization of TOM20 and FLAG from experiment in A (50 cells analyzed). (C) Mitochondria Proteinase K accessibility assay. Intact mitochondria (TRITON – and HEPES –), mitoplasts (TRITON – and HEPES +) or detergent solubilized mitochondria (TRITON + and HEPES +) from induced mitoBG4 cells were separated on SDS-PAGE. Antibody against mtSSB (mtDNA single strand DNA binding protein), OPA1 (Optic Atrophy 1) and TOM20 were used to detect mitochondrial matrix, inner mitochondrial membrane, and outer mitochondrial membrane respectively. (D) Immunoblot under native (– $\beta$ -mercaptoethanol) or reducing conditions (+ $\beta$ -mercaptoethanol) of recombinant BG4 protein (recBG4) or total cell extract from induced mitoBG4 cells (HEK mitoBG4) were separated on SDS-PAGE. Samples were probed with FLAG antibody to detect mitoBG4. Non-induced (–doxycycline) mitoBG4 cells were added as control.

toBG4 and mtSSB, another known nucleoid protein (Figure 2B and C).

To corroborate these results, we performed FLAG-immunoprecipitation after mitoBG4 expression. While the proteins of the mtDNA replisome and other mtDNA-interacting proteins (PRIMPOL and TFAM) co-precipitated with mitoBG4, we did not detect any interaction with the mitochondrial inner membrane protein OPA1 neither the cytosolic protein ACTIN nor the nuclear proteins PCNA and NUCLEOLIN (a nuclear DNA G4 binding protein (44)) (Figure 2D). Reciprocal immunoprecipitation with antibodies against mtDNA-binding proteins confirmed their interaction with mitoBG4 (Supplementary Figure S2). Notably, TOM20 was also detected in the mitoBG4 IP extract. This protein is required for mitochondrial import and apparently interacts with the non-processed form of mitoBG4 before it reaches the mitochondrial matrix (see Supplementary Figure S2A, note that mainly the higher MW band was detected in the bound fraction upon TOM20 IP).

We conclude that mitoBG4 directly interacts with the mitochondrial nucleoids.

#### mitoBG4 does not affect mtDNA maintenance

mitoBG4 expression in cells represents a feasible tool to detect endogenous mtDNA G4s formation only if its induction does not disrupt mtDNA maintenance or modifies G4 structure stability. It has been demonstrated that re-

combinant mitochondrial DNA polymerase  $\gamma$  (POLG) can pause DNA synthesis upon encountering G4 structures on the DNA template (11,45). However, the degree of pausing may vary depending on the specific G4 structure being tested (11). DNA polymerase stop assays using a previously tested mtDNA G4 template (Supplementary Figure S3A) (11) that has an anti-parallel topology (Supplementary Figure S3D and Supplementary Table S2) confirmed that G4 structures are an obstacle for POLG (Supplementary Figure S3B lanes 1 and 2). However, extended reaction times enabled POLG to partially bypass the G4 structure and synthesize a full-length run-off DNA product (Supplementary Figure S3B lane 3). The amount of pausing at the G4 structure can therefore be seen as a relative measurement of the G4 structure stability. In agreement with this, PhenDC3, a well-studied G4 stabilizer (25,46) reduced the full-length DNA to G4 pausing site ratio by  $\sim 80\%$  (Supplementary Figure S3C), whereas approximately 30% reduction was detected when using another stabilizer, RHPS4, indicating a weaker effect on G4 stabilization. This observation revealed that different compounds can alter the G4 bypassing activity of POLG to a different extent. In contrast, addition of recBG4 to the reaction, which binds the G4 structure (Supplementary Figure S3E), did not substantially alter the DNA products (Supplementary Figure S3C). The stalling of POLG is specific for the presence of the G4 structure, as the same reaction performed on a mtDNA sequence that did not contain a PGS did not result in any pausing of POLG (Supplementary Figure S3B, lanes 22–33).

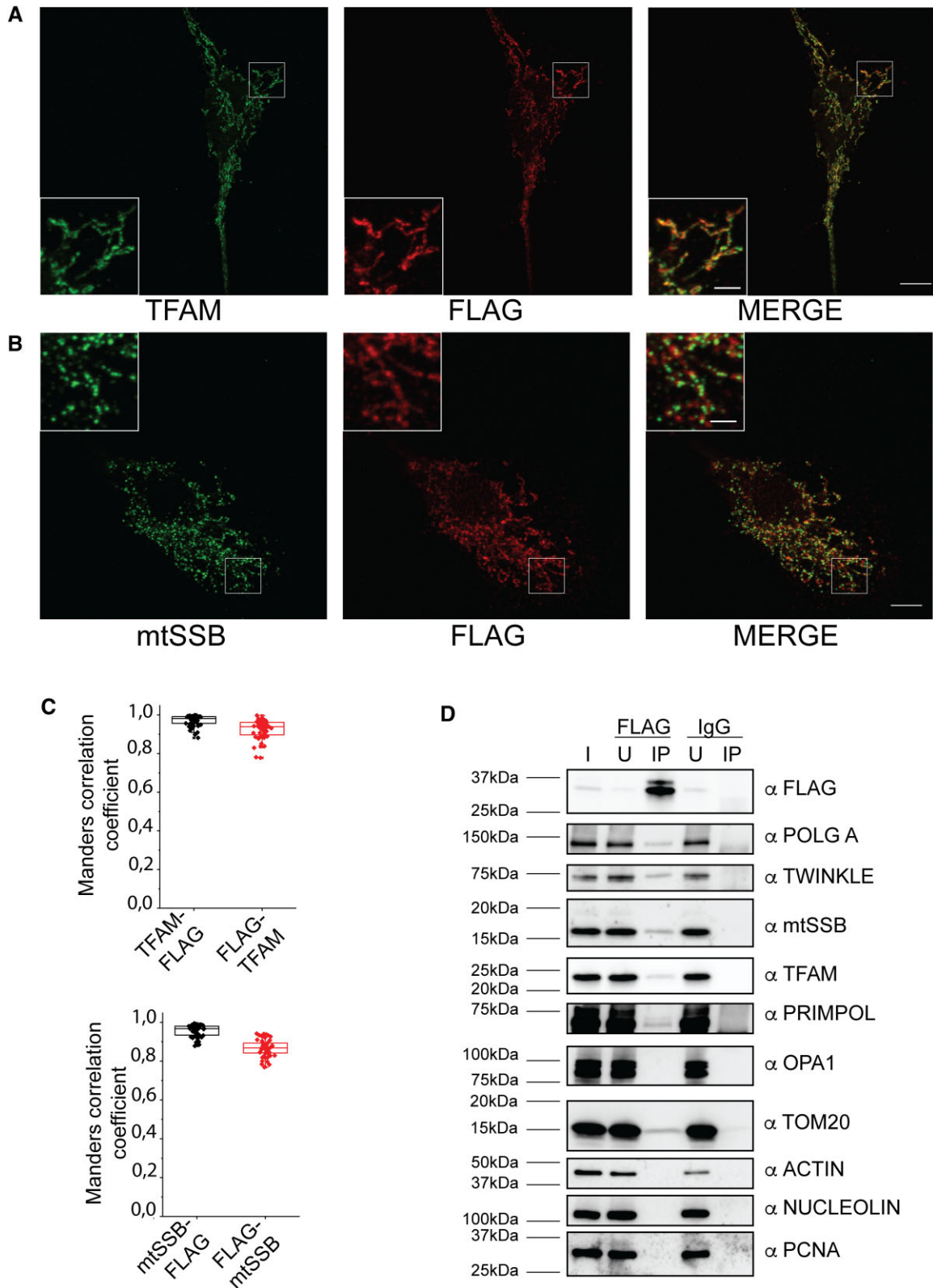


**Figure 2.** mitoBG4 interacts with mtDNA nucleoids. **A** and **B**. Representative immunofluorescence images of induced mitoBG4 cells immunolabeled with FLAG antibody (to detect mitoBG4) and TFAM (**A**) or mtSSB (**B**) antibodies. Scale bars: 10  $\mu$ m and 2  $\mu$ m in the magnified box. (**C**) Quantification of the reciprocal co-localization of nucleoid markers and FLAG from experiment in **A** (up-58 cells analyzed) and in **B** (bottom-48 cells analyzed). (**D**) Immunoblot of input (I), unbound (U) and pull-down (IP) fractions from FLAG and IgG immunoprecipitation of induced mitoBG4 cells. The blot was probed with the indicated antibodies. POLGA (mitochondrial Polymerase  $\gamma$ , subunit A) and the mitochondrial helicase TWINKLE are component of the mtDNA replication machinery; PRIMPOL is a primase-polymerase with mitochondrial localization. PCNA and NUCLEOLIN are nDNA binding proteins. ACTIN is a component of the cytoskeleton.

We conclude that BG4 binding to mtDNA is not likely to disrupt DNA synthesis by the major mitochondrial DNA polymerase POLG.

We then explored the effect of mitoBG4 expression on mtDNA in the mitoBG4 cells. Long-term treatment with doxycycline (up to 24 days) did not have any effect on the mtDNA copy number (Figure 3A and B). MtDNA copy number analysis might, however, not be able to detect mild interference of the mtDNA replication process. To address this more specifically, we performed two-dimensional agarose gel electrophoresis (2D-AGE) analysis of the mitochondrial DNA replication intermediates (26). The induction of mitoBG4 did not alter the pattern of mtDNA replication intermediates compared to control cells (Figure 3C and D).

Our findings suggest that BG4 is unlikely to significantly interfere with the progress of the mtDNA replication fork during replication and that its intracellular expression has no effect on the maintenance of mtDNA. This system can thus be used to detect the regions of mtDNA in which G4 structures are formed in human cells without affecting mtDNA metabolism.

#### mtG4-ChIP enriches for mtDNA G4 containing regions

We then set up a ChIP protocol to map the formation of G4s in the mitoBG4 cells by inducing the expression of mitoBG4 protein and subsequently performing a pull down with the FLAG antibody (mtG4-ChIP). To avoid alteration of the mitoBG4 binding to G4-DNA during the time of mitochondrial extraction (which can take up to several hours), we performed a cross-linking step on intact cells and sheared total genomic DNA (nDNA and mtDNA) from total cell extract (Supplementary Figure S4A). Optimal mtDNA shearing (fragment size between 500–300bp) was ensured by southern blot analysis with a mtDNA specific probe (ND5) (Supplementary Figure S4B). The FLAG pulldown extract and the INPUT samples were subsequently sent for next generation sequencing (NGS) using Illumina Platform.

We initially used a standard method for ChIP-seq analysis (33). However, we did not detect individual peaks for most of the samples (data not shown) probably because the Peak Calling MACS2 software was developed for nDNA analysis and might not take into consideration the multi-copy nature and the relatively small size of the mitochondrial genome. Therefore, to improve the visualization, we used a manual peak-calling methodology. Sequence analysis upon normalization showed several mtDNA regions enriched with respect to the INPUT (Figure 4A). The D-loop region was also enriched but was excluded from our analysis as this area was shown to be prone to artefacts in ChIP-seq protocols, as testified by enrichment upon pull down with IgG (47) or with uniquely localized nuclear transcription factors (48). We next performed mtG4-ChIP followed by qPCR (mtG4-ChIP-qPCR) and amplified two mtDNA regions that were enriched in all three replicates (Figure 4A and B). We detected 7-fold enrichment of these two regions compared to IgG, while no enrichment was detected for the cells that were not induced with doxycycline (i.e. no mitoBG4 expression) (Figure 4C). Our analysis of four nDNA regions, including three regions in the RPA3, CKD4 and

GAPDH genes that contain G4 structures and were previously reported as enriched in the total-genome G4-ChIP (15) showed no enrichment (Supplementary Figure S5A). This finding confirms that, in our cell model, mitoBG4 is uniquely localized in the mitochondria and mtG4-ChIP does not enrich for nDNA G4s. We also analyzed by mtG4-ChIP-qPCR two mtDNA regions that were not enriched in the ChIP-seq protocol, and we detected increased signal in the FLAG samples from induced cells, albeit to a lesser extent compared to the ChIP-seq enriched mtDNA regions (Supplementary Figure S5A). However, since PGS are dispersed throughout the mtDNA sequence (Figure 4A) and fragmentation of the mtDNA for the ChIP is always incomplete, even the less prevalent G4 structures will contribute to the overall mtDNA co-purification from cells expressing mitoG4.

We selected four G4HUNTER-predicted PGS which were located in the enriched regions in all three replicates and mapped within or in proximity (< 10nt) from the peak summit detected by MACS2 (Supplementary Table S1). Circular dichroism (CD) studies revealed that the selected PGS can fold into parallel G4 structures (positive ellipticity peak at 264nm, Supplementary Figure S6 and Supplementary Table S2). This applies also for mtDNA G4 9602 and mtDNA G4 13083, that, despite having an atypical G4 consensus sequence, fold into stable G4 structures as shown by the CD-melting and the K<sup>+</sup> dependency analysis (Supplementary Figure S7 and Supplementary Table S3). By contrast, scramble sequences with non-contiguous G-tracts did not display CD spectra indicative of any G4 topology (Supplementary Figure S6 and Supplementary Table S2). We then used electrophoretic mobility shift assay (EMSA) to evaluate the ability of recBG4 to bind these G4 structures *in vitro*. As expected, recBG4 bound to the G4 structures but was unable to bind to a mtDNA sequence that does not contain PGS (Supplementary Figure S6).

Taken together, these data suggest that mtDNA G4s are present in human cells under normal growth conditions and that mtG4-ChIP can be applied for their detection. However, the rather low level of G4 structures detected in mtDNA suggests that mtDNA G4s are transiently formed under normal cellular growth conditions.

#### mtG4-ChIP is specific for mtDNA

The nDNA is rich in sequences with high degree of homology with the mtDNA, the so called NUMTs (nuclear DNA mitochondrial sequences) (49). To confirm that the signal detected by mtG4-ChIP-seq protocol is specific for mtDNA and not the result of NUMTs pulldown, we depleted the mtDNA in the mitoBG4 cells by long-term ethidium bromide treatment (50). These cells are essentially  $\rho^0$  (i.e. devoid of mtDNA) as measured by qPCR amplifying two distinct regions of the mtDNA (Supplementary Figure S5B). We then performed the mtG4-ChIP-seq protocol on the mitoBG4  $\rho^0$  cells lines and detected no residual signal in the mtDNA upon pull down with the FLAG antibody (Supplementary Figure S5C), even though mitoBG4 was correctly processed and immunoprecipitated (Supplementary Figure S5D). These results, together with the lack of enrichment for nDNA G4 genes (Supplementary Figure S5A), confirm

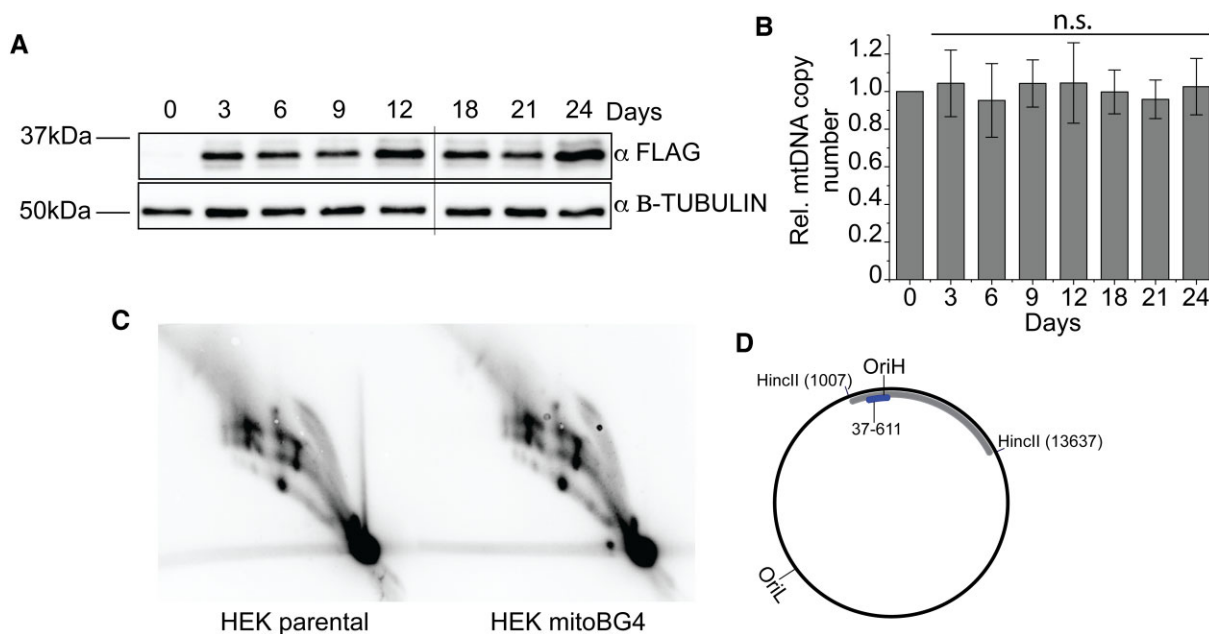


**Figure 3.** mitoBG4 does not affect mtDNA maintenance. (A) Immunoblot of total cell lysate from mitoBG4 cells induced with 10 ng/ml doxycycline for the indicated days. Anti B-TUBULIN was used as loading control. (B) mtDNA copy number of mitoBG4 cells induced with 10 ng/ml doxycycline for the indicated days. MtDNA copy number was determined by qPCR from total DNA. The relative mtDNA copy number was expressed as the ratio between mtDNA D-loop region and nuclear DNA B2M region and normalized to untreated samples. Data represent mean  $\pm$  s.d. of three independent experiments. Analysis of the data was performed with two-tail two samples *t*-test. n.s. = not significant. (C) 2D-AGE of HincII-digested mtDNA from parental HEK Flp-In T-REx cells transfected with the empty vector pcDNA5 (HEK parental) and induced HEK mitoBG4 cells (HEK mitoBG4), probed for the OriH-containing fragment as illustrated in (D). No differences in the replication intermediates can be observed. (D) A schematic illustration of human mtDNA showing the HincII restriction sites used for linearization of mtDNA. The probe used for Southern blot hybridization is indicated in blue.

that the signal detected in the normal cells by mtG4-ChIP-seq is specific for the mtDNA.

### Stabilization of mtDNA G4 interferes with mtDNA replication

Next, we investigated the consequence of G4 structures on the progression of the mtDNA replication fork. For this purpose, we took advantage of the known G4 stabilizer RHPS4 described to localize within the mitochondria and hypothesized to stabilize G4s in the mtDNA (51). We treated cells with 0.5  $\mu$ M RHPS4 and performed a time-dependent measurement of the mtDNA copy number. A clear decrease of mtDNA was observed in the presence of the G4-stabilizing compound compared to untreated cells, and after 24 hours mtDNA levels almost halved (Figure 5A), showing that RHPS4 essentially blocks the progression of mtDNA replication. In accordance, 2D-AGE analysis showed mtDNA replication intermediates accumulation, which is indicative of enhanced replication stalling (Supplementary Figure S8A-B-C). We did not detect accumulation of mtDNA deletions (Supplementary Figure S9A), which is in agreement with previous observations that show mtDNA deletions do not accumulate in actively proliferating cells (52).

To prove that the loss of mtDNA is a direct cause of enhanced G4 formation, we performed the mtG4-ChIP-seq protocol upon RHPS4 treatment. We treated induced mitoBG4 cells with 0.5  $\mu$ M RHPS4 for 3 h, when mtDNA copy number was not yet substantially affected (Figure 5A).

Analysis of the sequencing results revealed an overall strong increase in mtDNA sequence reads containing putative G4 sequences upon RHPS4 treatment (Figure 5B and C and Supplementary Table S4), indicating that RHPS4 causes stabilization of mtDNA G4s.

To confirm that RHPS4 enhances G4 stabilization without interfering with BG4 binding to G4 structures, we performed ELISA assay on an immobilized folded G4 sequence (12,42). While recBG4 exhibited specific binding to the G4 oligo (Supplementary Figure S8D), this binding was enhanced in the presence of RHPS4 (Supplementary Figure S8E). In contrast, when the G4 stabilizer PDS was present, the BG4 binding to the G4 structure was reduced, as previously reported (42).

Since we did not detect mtDNA deletions accumulation (Supplementary Figure S9A), we tested if copy number reduction was due to activation of mitophagy, a process implicated in clearing damaged mtDNA in dysfunctional mitochondria (52). RHPS4-mediated mtDNA G4 stabilization does not trigger mitophagy, as evidenced by unaltered steady-state mitochondrial protein levels (Supplementary Figure S9B) and lack of PINK1 recruitment to mitochondria (Supplementary Figure S9C) and LC-3 lipidation (Supplementary Figure S9D). Therefore, G4-dependent mtDNA copy number reduction is not driven by mitophagy activation.

We conclude that enhanced G4 formation blocks the progression of the mtDNA replication machinery and that mtG4-ChIP-seq is a suitable method to detect an increase in mtDNA G4 formation in human cell lines.

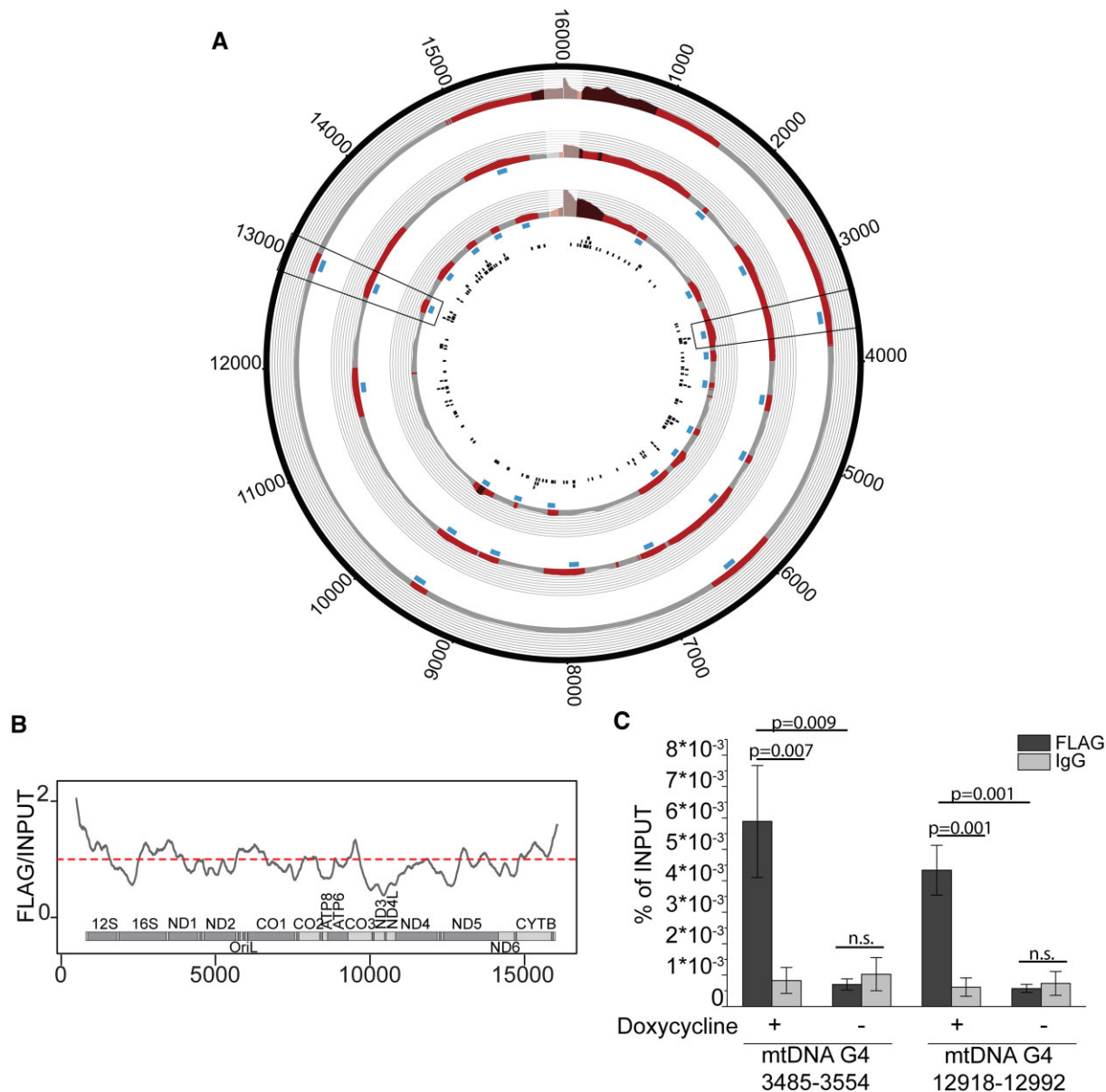


**Figure 4.** mtG4-ChIP enriches for mtDNA G4s. (A) mtG4-ChIP-seq profile for induced mitoBG4 cells pulled down with FLAG antibody. FLAG signal was normalized to the INPUT sample and expressed as ratio of FLAG versus INPUT. Areas in red indicate enrichment over INPUT samples (grey  $< 1$ , light red  $1 > x > 1.5$  and dark red  $> 1.5$ ). The blue boxes beneath the plots represent the narrow peaks that were extracted  $\pm 50$  bp from the max ratio of the enrichment range. The black boxes in the inner circle are predicted G4 sequences (using the G4Hunter algorithm). Three biological replicates are shown. D-loop region (in lighter color) was excluded from the analysis. The two black frames show the regions analyzed by ChIP-qPCR. (B) Linear plots showing the average FLAG to INPUT signal from the three replicates in (A). MtDNA sequence from nt 500 to nt 16 000 is displayed. (C) ChIP-qPCR upon pull down with FLAG antibody and IgG in induced (+) or non-induced (-) mitoBG4 cells. Data are expressed as % of INPUT pull down. Data represent mean  $\pm$  s.d. of three independent experiments. Analysis of the data was performed with two-tail two samples *t*-test. n.s. = not significant.

### Stalling of mtDNA replication enhances G-quadruplex formation in cultured human cells

We next asked whether G4 formation was altered when we disrupt the mtDNA replication process. The partially single-stranded nature of mtDNA replication intermediates could make them potentially prone to secondary DNA structure formation (e.g. G4s), especially when replication slows and exposes the GC-rich heavy strand for extended periods (53). To test whether impaired mtDNA replication has any impact on mtDNA G4s-formation,

we used the chain-terminating nucleoside analogue 2'-3'-dideoxycytidine (ddC) that is converted in the cell to ddCTP and it is specifically incorporated into mtDNA by POLG, resulting in mtDNA replication blockage due to chain termination (54). It is crucial to note that mtDNA replication restarts after ddCMP incorporation through a PRIMPOL-dependent pathway (24), with the DNA primer synthesized by PRIMPOL enabling POLG to continue replication. However, in the presence of ddCTP, POLG repeatedly terminates and restarts replication (with PRIMPOL assis-

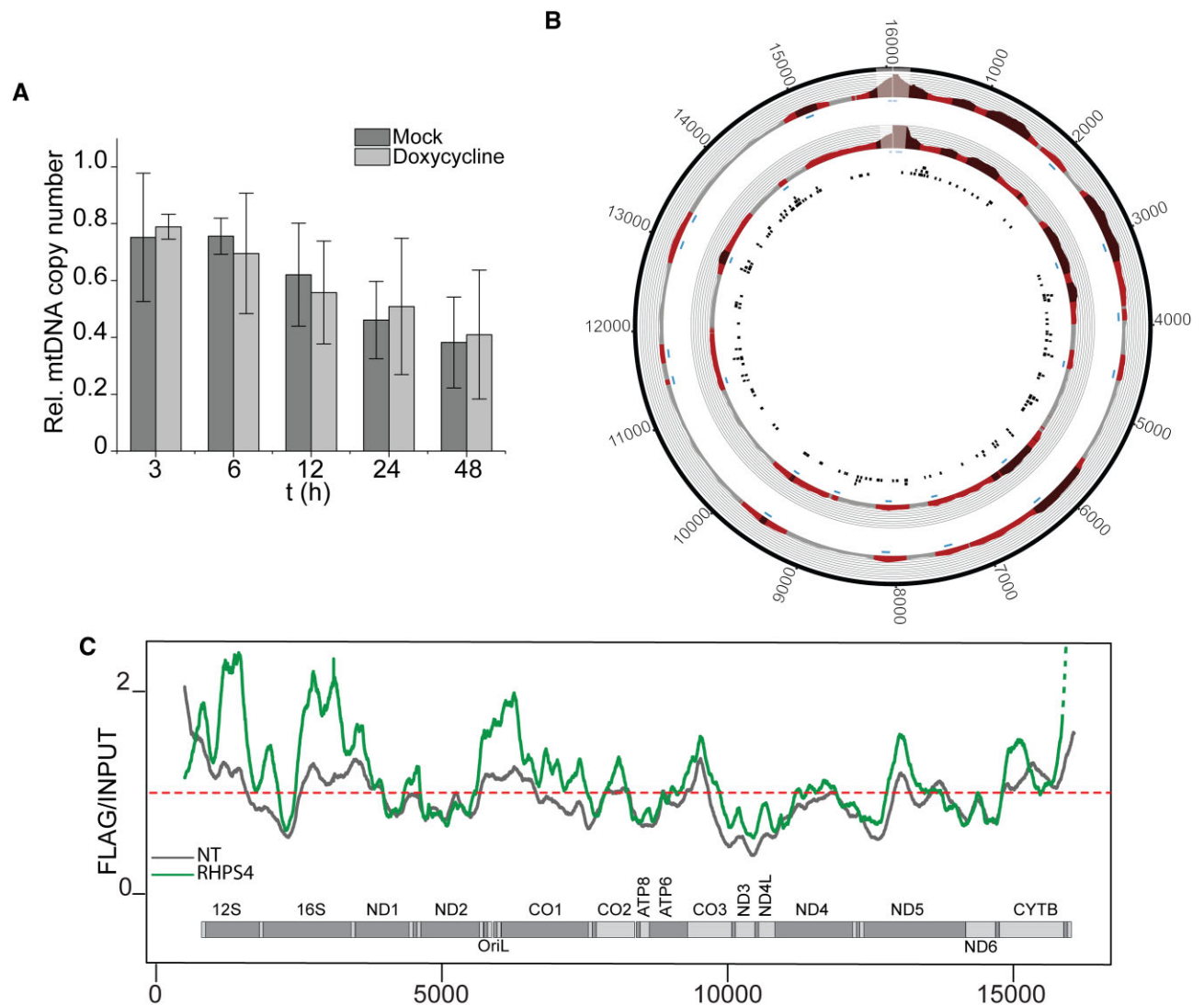


**Figure 5.** Stabilization of mtG4 causes increased mtG4-ChIP enrichment. (A) mtDNA copy number of induced mitoBG4 cells treated with 0.5  $\mu$ M RHPS4 for the indicated time points. MtDNA copy number was determined by qPCR from total DNA. The relative mtDNA copy number was expressed as the ratio between mtDNA D-loop region and nuclear DNA  $\beta$ 2M region and normalized to untreated samples. Data represent mean  $\pm$  s.d. of three independent experiments. (B) mtG4-ChIP-seq profile for induced mitoBG4 cells treated with 0.5  $\mu$ M RHPS4 for 3 h before pulling down with FLAG antibody. FLAG signal was normalized to the INPUT sample and expressed as ratio of FLAG vs INPUT. Areas in red indicate enrichment over INPUT samples (grey < 1, light red 1 >  $x$  > 1.5 and dark red > 1.5). The blue boxes beneath the plots represent the narrow peaks that were extracted  $\pm$ 50 bp from the max ratio of the enrichment range. The black boxes in the inner circle are predicted G4 sequences (using the G4Hunter algorithm). Two technical replicates are shown. (C) Linear plots showing the average FLAG to INPUT signal from the doxycycline induced replicates (in grey) and RHPS4 treated replicates (in green). MtDNA sequence from nt 500 to nt 16 000 is displayed.

tance) due to the competing concentrations of ddCTP and the endogenous dCTP, resulting in a cycle referred to as stall/slowing of the replication process.

We induced the expression of mitoBG4 in combination with the addition of ddC using conditions (ddC, 200  $\mu$ M and 3 h) that ensures minimal mtDNA copy number loss (Figure 6A) but also apparent accumulation of stalled mtDNA replication forks (26), and performed the mtG4-ChIP-seq (Supplementary Figure S10A). Compared to normal growth conditions, we detected an increase in the enrichment of some of the mtDNA G4 regions in ddC-treated cells (Supplementary Figure S10B and Supplementary Table S4). This modest ddC-induced increase of the mtG4-

ChIP-seq signal suggests that slowed mtDNA replication might account for enhanced G4 formation on the mitochondrial genome.

To increase the amount of mtDNA molecules that show replication stalling, we tested the effect of longer ddC treatment (12 h and 24 h) and performed mtG4-ChIP-qPCR in mitoBG4-expressing cells. Interestingly the ddC-dependent increase of G4 detection after prolonged treatment was more pronounced on the major arc region (12 928–12 992 nt), compared to the minor arc region (3845–3554 nt) (Figure 6B). No enrichment was detected at nDNA G4 regions (Supplementary Figure S10C) nor upon pull-down with IgG (Figure 6B), confirming the specificity of mtG4-

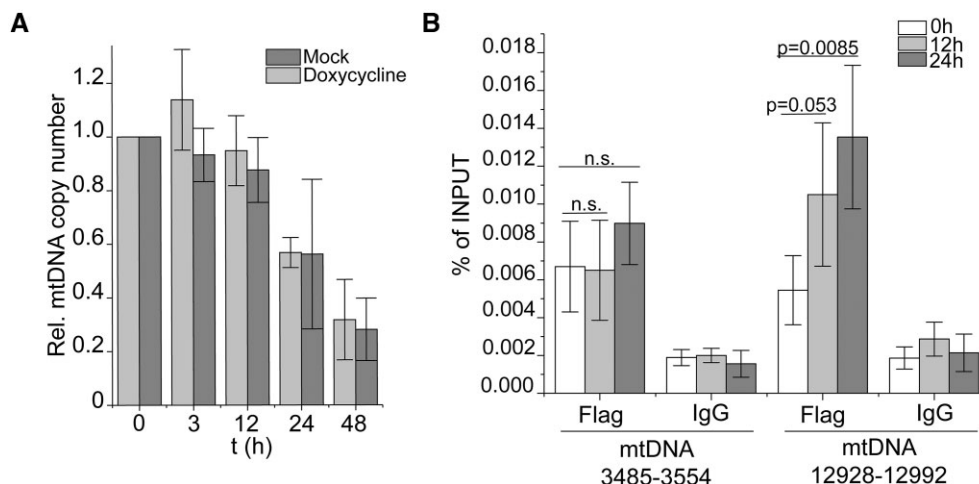


**Figure 6.** Effect of stalling of the mtDNA machinery in mtDNA G4 formation. (A) mtDNA copy number of induced mitoBG4 cells treated with 200  $\mu$ M ddC for the indicated time points. MtDNA copy number was determined by qPCR from total DNA. The relative mtDNA copy number was expressed as the ratio between mtDNA D-loop region and nuclear DNA B2M region and normalized to untreated samples. Data represent mean  $\pm$  s.d. of three independent experiments. (B) ChIP-qPCR upon pull down with FLAG antibody or mouse IgG in induced mitoBG4 cells treated with 200  $\mu$ M ddC for the indicated time points. Data are expressed as % of INPUT and represent mean  $\pm$  s.d. of four independent experiments. Analysis of the data was performed using the two-tail two samples t-test. n.s. = not significant.

ChIP and of the ddC treatment for mtDNA. These data are consistent with enhanced G4 formation on the exposed parental ssDNA H-strand due to a slow progressing mtDNA replication machinery (stalling) during strand-asynchronous mtDNA replication.

To demonstrate that increased ssDNA formation enhances mtDNA G4 accumulation, we transiently overexpressed the replicative helicase TWINKLE in mitoBG4 cells (Supplementary Figure S10D), which boosts mtDNA replication (55,56). TWINKLE over-expression increased mtDNA G4 levels, with a stronger signal in the 12928–12992 region than the 3485–3554 region (Supplementary Figure S10E and S10F). In contrast, POLG overexpression (Supplementary Figure S10D), that does not increase mtDNA replication (26), had no impact on G4 formation (Supplementary Figure S10E).

These experiments indicate that mitochondrial G4 structures primarily form during the replication process when single-stranded DNA (ssDNA) intermediates are present, especially on the major arc, which remains single-stranded for an extended period during strand-displacement replication.

## DISCUSSION

In this study, we developed a cell model that allows the detection and mapping of G4s specifically in the mtDNA of human cell lines, by targeting the G4-binding synthetic antibody BG4 to mitochondria.

About 99% of the mitochondrial proteome is encoded by the nDNA and translated by cytoplasmic ribosomes in the form of precursor proteins that are subsequently imported inside the mitochondria. A far majority of proteins that localizes in the mitochondrial matrix, including the components of the mtDNA replisomes, contains an N-terminal sequence that allows for recognition by specific translocases of the mitochondrial outer and inner mem-

branes that drive the import inside the organelles. Once the precursor protein reaches the mitochondrial matrix the N-terminal targeting sequence is cleaved off by specific mitochondrial proteases (57). The targeting of heterologous protein inside the mitochondria, by fusing the protein of interest with the N-terminal targeting sequence from nuclear-encoded proteins with known mitochondrial localization, is a widely exploited strategy to target bacterial or artificial nucleases (58–61) with the purpose of editing the mitochondrial genome. In here, we employed this strategy to drive BG4 inside the mitochondria.

We proved that mitoBG4 is correctly localized and folded within the mitochondrial matrix. Moreover, inside the organelle, mitoBG4 interacts with the mtDNA without interfering with the process of mtDNA replication. We subsequently developed a chromatin immunoprecipitation approach specific for mtDNA (mtG4-ChIP) coupled with sequencing that allowed us to detect G4 formation in human cells. Our results showed that the mtG4-ChIP-seq not only enriches mtDNA sequences that have the ability to form G4s *in vitro*, but also demonstrates that the level of mtDNA G4 structures is low under regular cell culture conditions, which is in line with the idea that G4s on the mtDNA are transient in nature. To further validate our approach, we employed RHPS4, a well-recognized G4-stabilizing compound, and detected substantial increase of mtDNA G4 formation in cells after its addition. Furthermore, this increase in mitochondrial G4s leads to a rapid loss of mtDNA, indicating that elevated levels of G4s block the progression of the mtDNA replication fork. In addition, ddC-induced mtDNA replication stalling increases G4 detection by mtG4-ChIP, particularly in the major arc of the mtDNA, suggesting that a slower mtDNA duplication process and/or increase exposure of ssDNA enhances G4 formation specifically in the region of the mitochondrial genome where mtDNA deletions accumulate in disease.

The mtG4-ChIP method represents a novel and unique tool to study the dynamics of G4 structures in the mtDNA. In contrast to a previously described G4-ChIP method (14), in which BG4 binding to the G4 structures is performed on DNA samples that underwent several manipulation procedures including detergent treatment, fixation and DNA shearing that might cause distortion of the G4 structures and or epitope masking (during fixation), in the mtG4-ChIP method, BG4 is expressed in the cells and binds to G4 structures in the living cells prior to the downstream procedures required by the ChIP protocol.

Although it is theoretically possible that BG4 binding to mtDNA captures mtDNA G4 structures undergoing dynamic interconversion with other structural states, favoring G4-folded structures, the observation that mtG4-ChIP-seq detects changes in G4 intensity and location dependent on different drug treatments (RHPS4 or ddC) argues against the mapped G4 structures being a systematic artefact caused by antibody binding.

Human mtDNA, despite being small in size, is highly enriched in putative G4-forming sequences, with a frequency of 6.6 G4s for every 1000 nts, as detected using the G4Hunter software (62). However, the amount of mtDNA G4s detected under normal cell culture conditions is limited. This could be explained by the fact that the formation of G4s in the mtDNA under physiological conditions is prevented by the function of the mtDNA replisome (and the coating by mtSSB) and/or by the action of specific proteins (e.g. the helicases PIF1 and REQL4 or the nuclease helicase DNA2 (63)) in charge of their clearance.

These experimental findings, implying limited formation of mtDNA G4 structures and the absence of specific hotspots for their formation, reflect the observations in patients with mtDNA deletions accumulation. Indeed, most patients, while carrying the genetic defects from birth, usually present with the first symptoms of the disease in adulthood, indicating that the accumulation of mtDNA deletions is a slow process rather than an acute event. In addition, the pattern of deletions found in these patients is extremely variable, and it does not only differ between different patients, but also in different tissues within the same patient (64,65).

Under normal growth conditions, the formation of mtDNA G4s, as detected by mtG4-ChIP-seq, is more prevalent in the region between 0 and 6000 nts, and this is further increased upon treatment with the G4 stabilizer (RHPS4). These data correlate with previous transcriptomic analysis on RHPS4-treated cells presenting with a progressive decrease of transcripts originating from HSP promoters (51). Since these transcripts are transcribed from the H-strand, this observation is consistent with the increased amount of G4 formation that we detect in the H-strand downstream of HSP (Figure 7A). Thus, under normal cellular conditions, G4s might transiently form in the mtDNA during mitochondrial transcription, but their short-lived presence may not affect the ability of the mitochondrial replication fork to duplicate the mtDNA. However, the persistence of these structures by the interaction with a G4 stabilizer (RHPS4) will lead to reduced transcription and subsequent block of mtDNA replication, resulting in genetic instability. In agreement with this, Butler and co-

workers demonstrated that DNA synthesis by two known mitochondrial DNA polymerases (POLG and PRIMPOL) *in vitro* was strongly blocked by stable G4 structures (45).

In contrast to the RHPS4 effect, stalling of the DNA replisome induced by the POLG-specific inhibitor ddC revealed enhanced formation of G4 in the major arc of the mtDNA. Human mtDNA replication occurs in a highly strand-asynchronous manner such that the lagging strand (L-strand) is synthesized with considerable delay. The implication of this mode of replication is that the parental H-strand is exposed in single-stranded form for an extended period of time (Figure 7B). The single-stranded nature of the parental H-strand could make it more prone to G4 formation, in particular when replication moves slowly and the major arc of the parental H-strand is exposed even longer than under normal conditions. The slower movement of the replication machinery could be due to the presence of ddC, as in Figure 6B, or to defects in replisome components, as we and others have previously shown that a defective mitochondrial replication machinery can cause slowing of the replication process (26,66,67). This could also explain why most mtDNA deletion breakpoints in patients have been mapped within the major arc where the replication machinery will more likely be challenged by G4 formation. The G4s formed on the exposed parental H-strand will not hamper nascent H-strand synthesis that uses the parental L-strand as template, but the structures will be encountered during the synthesis of the nascent L-strand. This is compatible with the recently proposed mechanism of mtDNA deletion formation through copy-choice recombination during L-strand synthesis (68). In short, G4s can form a replication barrier, causing dissociation of POLG during synthesis of the nascent L-strand. DNA breathing could allow re-annealing of the 3' end of the nascent L-strand DNA at a complementary downstream sequence on the parental H-strand, explaining why G4-forming sequences are enriched at mtDNA deletion breakpoints.

As mentioned earlier, ddC increases ssDNA mtDNA replication intermediates in cells, which we hypothesize results in a higher mtG4-ChIP signal, suggesting that mtDNA G4s are more prevalent in actively replicating mtDNA molecules compared to those that are not replicating. Indeed, we observed mtDNA G4 increase when enhancing mtDNA replication via TWINKLE over-expression (Supplementary Figure S10E), supporting the idea that mitochondrial G4 formation in mitochondria is more likely to occur during the replication process.

Overall, our data and work from others indicate that while G4-forming sequences evolved in the mtDNA genome with a role in regulating transcription and translation (5–7), they do not represent a threat for the progression of the mtDNA replication machinery under normal conditions. However, they could potentially have a negative impact on mtDNA stability when other factors interfere with the process of mtDNA replication.

Taken together, these data indicate that we can now visualize mtDNA G4s formed in cultured human cells without perturbing their dynamics. The mtG4-ChIP protocol will be instrumental in future research to identify the factors affecting G4 formation in mtDNA, the helicases and nucleases involved in their resolution and, ultimately, to understand

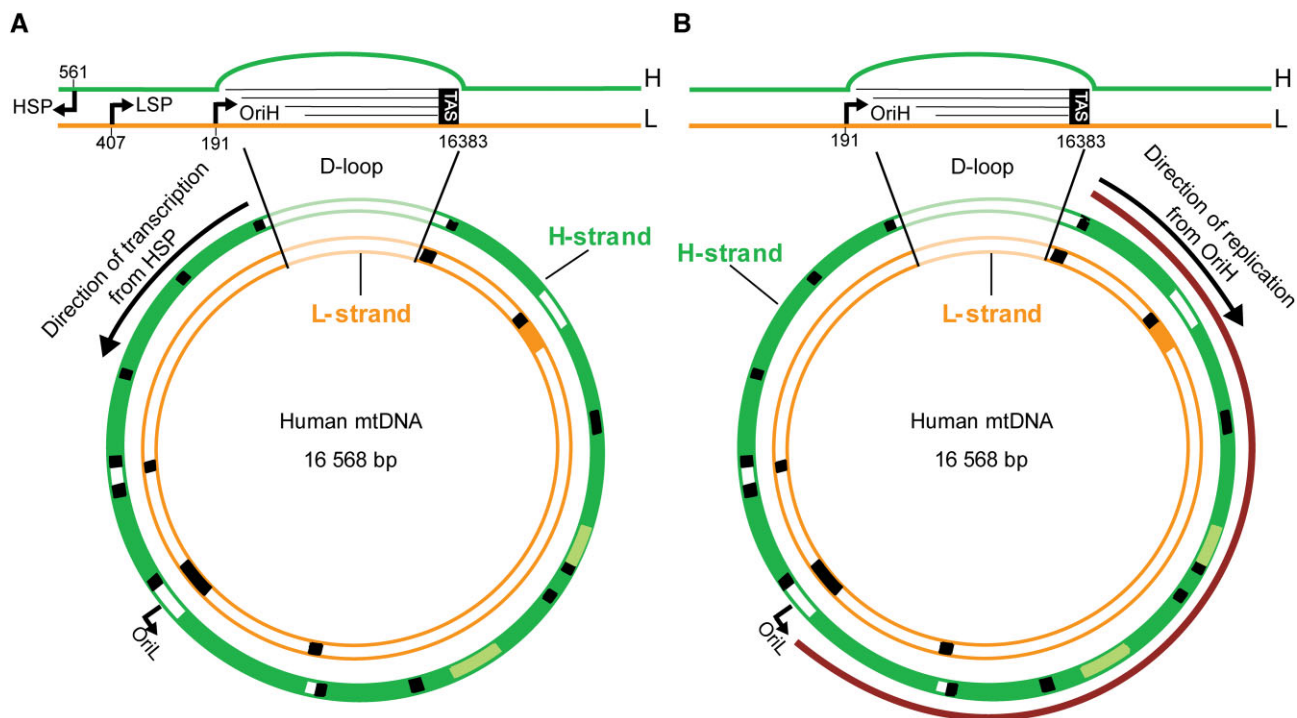


**Figure 7.** Schematic representation of the human mtDNA including the direction of mtDNA transcription (A) and replication (B). mtDNA is represented anti-clockwise. mtDNA transcription of the H-strand occurs in anti-clockwise direction (black arrow in A). mtDNA DNA replication of the H-strand occurs in clockwise direction (black arrow in B). The control region (D-loop) is depicted in more details. Green: heavy strand (H-strand); orange: light strand (L-strand); red: major arc. OriH and OriL are the origins of replication for heavy and light strand respectively. HSP: H-strand promoter for transcription; LSP: L-strand promoter for transcription. TAS: termination associated-sequences.

the mechanistic role of G4s in the generation of pathogenic mtDNA deletions.

#### DATA AVAILABILITY

The ChIP-seq data have been deposited to the Sequence Read Archive (SRA) at NCBI (<https://www.ncbi.nlm.nih.gov/sra>) under the accession number PRJNA811445.

#### SUPPLEMENTARY DATA

[Supplementary Data](#) are available at NAR Online.

#### ACKNOWLEDGEMENTS

We acknowledge Irene Martinez Carrasco and the Biochemical Imaging Centre at Umeå University and the National Microscopy infrastructure, NMI [VR-RFI 2019–00217], for providing assistance. We thank Shankar Balasubramanian (Cancer Research UK Cambridge Institute, UK) for providing the pSANG10-3F-BG4 plasmid and Mikeal Lindberg and the Protein Expertise Platform (PEP-Umeå University) for purification of recBG4. We thank Hans Spelbrink (Radboud Center for Mitochondrial Medicine, The Netherlands) for providing the pCDNA 3.1 POLG and TWINKLE plasmids. We thank Jan Jamroskovic (Nasim Sabouri Lab, Umeå University) and Dale Corkery (Yaowen Wu Lab, Umeå University) for sharing reagents. We thank Paulina Wanrooij, Josefin Forslund, Gorazd Stojkovic and Xin Zhou for the helpful discussion.

We finally acknowledge Paolo Lorenzon for helping in the preparation of the figures.

#### FUNDING

Knut and Alice Wallenberg Foundation [to S.W.]; Swedish Research Council [VR-MH 2018-0278 to S.W., VR-NT 2017-05235 to E.C.]; Kempe foundations [SMK-1632 to E.C.]; Wenner-Gren Foundations [to S.W. and M.D.]; HORIZON 2020 Framework Programme-H2020 Marie Skłodowska-Curie Actions [751474 to M.D.]; PNRR-Young Researcher MSCA program, Italian Ministry of University and Research [to M.D.]; Swedish Foundation for Strategic Research [RIF14-0081 to M.D.L.]; Finnish Academy [332458 to S.G., 338227 to J.L.O.P.]. Funding for open access charge: Swedish Research Council [VR-MH 2018-0278 to S.W.].

*Conflict of interest statement.* None declared.

#### REFERENCES

- Doimo, M., Pfeiffer, A., Wanrooij, P.H. and Wanrooij, S. (2020) Gasparre, G. and Porcelli, A.M. (ed.) *The Human Mitochondrial Genome*. Academic Press, pp. 3–33.
- El-Hattab, A.W., Craigen, W.J. and Scaglia, F. (2017) Mitochondrial DNA maintenance defects. *Biochim. Biophys. Acta Mol. Basis Dis.*, **1863**, 1539–1555.
- Chambers, V.S., Marsico, G., Boutell, J.M., Di Antonio, M., Smith, G.P. and Balasubramanian, S. (2015) High-throughput sequencing of DNA G-quadruplex structures in the human genome. *Nat. Biotechnol.*, **33**, 877–881.

4. Rhodes, D. and Lipps, H.J. (2015) G-quadruplexes and their regulatory roles in biology. *Nucleic Acids Res.*, **43**, 8627–8637.
5. Wanrooij, P.H., Uhler, J.P., Simonsson, T., Falkenberg, M. and Gustafsson, C.M. (2010) G-quadruplex structures in RNA stimulate mitochondrial transcription termination and primer formation. *Proc. Natl. Acad. Sci. U.S.A.*, **107**, 16072–16077.
6. Wanrooij, P.H., Uhler, J.P., Shi, Y., Westerlund, F., Falkenberg, M. and Gustafsson, C.M. (2012) A hybrid G-quadruplex structure formed between RNA and DNA explains the extraordinary stability of the mitochondrial R-loop. *Nucleic Acids Res.*, **40**, 10334–10344.
7. Pietras, Z., Wojcik, M.A., Borowski, L.S., Szewczyk, M., Kulinski, T.M., Cysewski, D., Stepien, P.P., Dziembowski, A. and Szczesny, R.J. (2018) Dedicated surveillance mechanism controls G-quadruplex forming non-coding RNAs in human mitochondria. *Nat. Commun.*, **9**, 2558.
8. Dong, D.W., Pereira, F., Barrett, S.P., Kolesar, J.E., Cao, K., Damas, J., Yatsunyk, L.A., Johnson, F.B. and Kaufman, B.A. (2014) Association of G-quadruplex forming sequences with human mtDNA deletion breakpoints. *BMC Genomics [Electronic Resource]*, **15**, 677.
9. Bharti, S.K., Sommers, J.A., Zhou, J., Kaplan, D.L., Spelbrink, J.N., Mergny, J.L. and Brosh, R.M. Jr. (2014) DNA sequences proximal to human mitochondrial DNA deletion breakpoints prevalent in human disease form G-quadruplexes, a class of DNA structures inefficiently unwound by the mitochondrial replicative Twinkle helicase. *J. Biol. Chem.*, **289**, 29975–29993.
10. Tarsounas, M. and Tijsterman, M. (2013) Genomes and G-quadruplexes: for better or for worse. *J. Mol. Biol.*, **425**, 4782–4789.
11. Sullivan, E.D., Longley, M.J. and Copeland, W.C. (2020) Polymerase gamma efficiently replicates through many natural template barriers but stalls at the HSP1 quadruplex. *J. Biol. Chem.*, **295**, 17802–17815.
12. Biffi, G., Tannahill, D., McCafferty, J. and Balasubramanian, S. (2013) Quantitative visualization of DNA G-quadruplex structures in human cells. *Nat. Chem.*, **5**, 182–186.
13. Laguerre, A., Hukezalie, K., Winckler, P., Katranji, F., Chanteloup, G., Pirrotta, M., Perrier-Cornet, J.M., Wong, J.M. and Monchaud, D. (2015) Visualization of RNA-Quadruplexes in Live Cells. *J. Am. Chem. Soc.*, **137**, 8521–8525.
14. Hänsel-Hertsch, R., Beraldi, D., Lensing, S.V., Marsico, G., Zyner, K., Parry, A., Di Antonio, M., Pike, J., Kimura, H., Narita, M. et al. (2016) G-quadruplex structures mark human regulatory chromatin. *Nat. Genet.*, **48**, 1267–1272.
15. Hänsel-Hertsch, R., Spiegel, J., Marsico, G., Tannahill, D. and Balasubramanian, S. (2018) Genome-wide mapping of endogenous G-quadruplex DNA structures by chromatin immunoprecipitation and high-throughput sequencing. *Nat. Protoc.*, **13**, 551–564.
16. Lyu, J., Shao, R., Kwong Yung, P.Y. and Elsässer, S.J. (2022) Genome-wide mapping of G-quadruplex structures with CUT&Tag. *Nucleic Acids Res.*, **50**, e13.
17. Shivalingam, A., Izquierdo, M.A., Marois, A.L., Vyšniauskas, A., Suhling, K., Kuimova, M.K. and Vilar, R. (2015) The interactions between a small molecule and G-quadruplexes are visualized by fluorescence lifetime imaging microscopy. *Nat. Commun.*, **6**, 8178.
18. Summers, P.A., Lewis, B.W., Gonzalez-Garcia, J., Porreca, R.M., Lim, A.H.M., Cadinu, P., Martin-Pintado, N., Mann, D.J., Edel, J.B., Vannier, J.B. et al. (2021) Visualising G-quadruplex DNA dynamics in live cells by fluorescence lifetime imaging microscopy. *Nat. Commun.*, **12**, 162.
19. Suseela, Y.V., Narayanaswamy, N., Pratihari, S. and Govindaraju, T. (2018) Far-red fluorescent probes for canonical and non-canonical nucleic acid structures: current progress and future implications. *Chem. Soc. Rev.*, **47**, 1098–1131.
20. Di Antonio, M., Ponjavic, A., Radzevičius, A., Ranasinghe, R.T., Catalano, M., Zhang, X., Shen, J., Needham, L.M., Lee, S.F., Klenerman, D. et al. (2020) Single-molecule visualization of DNA G-quadruplex formation in live cells. *Nat. Chem.*, **12**, 832–837.
21. Hu, M.H. (2021) Molecular engineering of a near-infrared fluorescent ligand for tracking mitochondrial DNA G-quadruplexes. *Anal. Chim. Acta*, **1169**, 338600.
22. Chen, X.C., Tang, G.X., Luo, W.H., Shao, W., Dai, J., Zeng, S.T., Huang, Z.S., Chen, S.B. and Tan, J.H. (2021) Monitoring and Modulating mtDNA G-Quadruplex Dynamics Reveal Its Close Relationship to Cell Glycolysis. *J. Am. Chem. Soc.*, **143**, 20779–20791.
23. Guo, X., Chen, H., Liu, Y., Yang, D., Li, Q., Du, H., Liu, M., Tang, Y. and Sun, H. (2022) An organic molecular compound for in situ identification of mitochondrial G-quadruplexes in live cells. *J. Mater. Chem. B*, **10**, 430–437.
24. Torregrosa-Munumer, R., Forslund, J.M.E., Goffart, S., Pfeiffer, A., Stojkovic, G., Carvalho, G., Al-Furoukh, N., Blanco, L., Wanrooij, S. and Pohjoismaki, J.L.O. (2017) PrimPol is required for replication reinitiation after mtDNA damage. *Proc. Natl. Acad. Sci. U.S.A.*, **114**, 11398–11403.
25. Prasad, B., Doimo, M., Andréasson, M., L'Hôte, V., Chorell, E. and Wanrooij, S. (2022) A complementary chemical probe approach towards customized studies of G-quadruplex DNA structures in live cells. *Chem. Sci.*, **13**, 2347–2354.
26. Wanrooij, S., Goffart, S., Pohjoismaki, J.L., Yasukawa, T. and Spelbrink, J.N. (2007) Expression of catalytic mutants of the mtDNA helicase Twinkle and polymerase POLG causes distinct replication stalling phenotypes. *Nucleic Acids Res.*, **35**, 3238–3251.
27. Jamroskovic, J., Doimo, M., Chand, K., Obi, I., Kumar, R., Brannstrom, K., Hedenstrom, M., Nath Das, R., Akhunjyan, A., Deiana, M. et al. (2020) Quinazoline Ligands Induce Cancer Cell Death through Selective STAT3 Inhibition and G-Quadruplex Stabilization. *J. Am. Chem. Soc.*, **142**, 2876–2888.
28. Bolte, S. and Cordelieres, F.P. (2006) A guided tour into subcellular colocalization analysis in light microscopy. *J. Microsc.*, **224**, 213–232.
29. Schneider, C.A., Rasband, W.S. and Eliceiri, K.W. (2012) NIH Image to ImageJ: 25 years of image analysis. *Nat. Methods*, **9**, 671–675.
30. Phillips, N.R., Sprouse, M.L. and Roby, R.K. (2014) Simultaneous quantification of mitochondrial DNA copy number and deletion ratio: a multiplex real-time PCR assay. *Sci. Rep.*, **4**, 3887.
31. Forslund, J.M.E., Pfeiffer, A., Stojkovic, G., Wanrooij, P.H. and Wanrooij, S. (2018) The presence of rNTPs decreases the speed of mitochondrial DNA replication. *PLoS Genet.*, **14**, e1007315.
32. Wanrooij, S., Miralles Fuste, J., Stewart, J.B., Wanrooij, P.H., Samuelsson, T., Larsson, N.G., Gustafsson, C.M. and Falkenberg, M. (2012) In vivo mutagenesis reveals that OriL is essential for mitochondrial DNA replication. *EMBO Rep.*, **13**, 1130–1137.
33. Afgan, E., Baker, D., van den Beek, M., Blankenberg, D., Bouvier, D., Čech, M., Chilton, J., Clements, D., Coraor, N., Eberhard, C. et al. (2016) The Galaxy platform for accessible, reproducible and collaborative biomedical analyses: 2016 update. *Nucleic Acids Res.*, **44**, W3–W10.
34. Li, H. and Durbin, R. (2009) Fast and accurate short read alignment with Burrows-Wheeler transform. *Bioinformatics*, **25**, 1754–1760.
35. Landt, S.G., Marinov, G.K., Kundaje, A., Kheradpour, P., Pauli, F., Batzoglou, S., Bernstein, B.E., Bickel, P., Brown, J.B., Cayting, P. et al. (2012) ChIP-seq guidelines and practices of the ENCODE and modENCODE consortia. *Genome Res.*, **22**, 1813–1831.
36. Kharchenko, P.V., Tolstorukov, M.Y. and Park, P.J. (2008) Design and analysis of ChIP-seq experiments for DNA-binding proteins. *Nat. Biotechnol.*, **26**, 1351–1359.
37. Jun, G., Wing, M.K., Abecasis, G.R. and Kang, H.M. (2015) An efficient and scalable analysis framework for variant extraction and refinement from population-scale DNA sequence data. *Genome Res.*, **25**, 918–925.
38. Breese, M.R. and Liu, Y. (2013) NGSUtils: a software suite for analyzing and manipulating next-generation sequencing datasets. *Bioinformatics*, **29**, 494–496.
39. Ramirez, F., Ryan, D.P., Gruning, B., Bhardwaj, V., Kilpert, F., Richter, A.S., Heyne, S., Dundar, F. and Manke, T. (2016) deepTools2: a next generation web server for deep-sequencing data analysis. *Nucleic Acids Res.*, **44**, W160–W165.
40. 1000 Genome Project Data Processing Subgroup, Li, H., Handsaker, B., Wysoker, A., Fennell, T., Ruan, J., Homer, N., Marth, G., Abecasis, G. and Durbin, R. (2009) The Sequence Alignment/Map format and SAMtools. *Bioinformatics*, **25**, 2078–2079.
41. Krzywinski, M., Schein, J., Birol, I., Connors, J., Gascoyne, R., Horsman, D., Jones, S.J. and Marra, M.A. (2009) Circos: an information aesthetic for comparative genomics. *Genome Res.*, **19**, 1639–1645.
42. Masson, T., Landras Guetta, C., Laigre, E., Cucchiari, A., Duchambon, P., Teulade-Fichou, M.P. and Verga, D. (2021) BrdU immuno-tagged G-quadruplex ligands: a new ligand-guided immunofluorescence approach for tracking G-quadruplexes in cells. *Nucleic Acids Res.*, **49**, 12644–12660.
43. Pohjoismaki, J.L., Wanrooij, S., Hyvarinen, A.K., Goffart, S., Holt, I.J., Spelbrink, J.N. and Jacobs, H.T. (2006) Alterations to the expression

- level of mitochondrial transcription factor A, TFAM, modify the mode of mitochondrial DNA replication in cultured human cells. *Nucleic Acids Res.*, **34**, 5815–5828.
44. Gonzalez, V., Guo, K., Hurley, L. and Sun, D. (2009) Identification and characterization of nucleolin as a c-myc G-quadruplex-binding protein. *J. Biol. Chem.*, **284**, 23622–23635.
  45. Butler, T.J., Estep, K.N., Sommers, J.A., Maul, R.W., Moore, A.Z., Bandinelli, S., Cucca, F., Tuke, M.A., Wood, A.R., Bharti, S.K. *et al.* (2020) Mitochondrial genetic variation is enriched in G-quadruplex regions that stall DNA synthesis in vitro. *Hum. Mol. Genet.*, **29**, 1292–1309.
  46. De Cian, A., Delemos, E., Mergny, J.L., Teulade-Fichou, M.P. and Monchaud, D. (2007) Highly efficient G-quadruplex recognition by bisquaterninium compounds. *J. Am. Chem. Soc.*, **129**, 1856–1857.
  47. Inatomi, T., Matsuda, S., Ishiuchi, T., Do, Y., Nakayama, M., Abe, S., Kasho, K., Wanrooij, S., Nakada, K., Ichiyanagi, K. *et al.* (2022) TFB2M and POLRMT are essential for mammalian mitochondrial DNA replication. *Biochim. Biophys. Acta Mol Cell Res.*, **1869**, 119167.
  48. Marinov, G.K., Wang, Y.E., Chan, D. and Wold, B.J. (2014) Evidence for site-specific occupancy of the mitochondrial genome by nuclear transcription factors. *PLoS One*, **9**, e84713.
  49. Bensasson, D., Zhang, D., Hartl, D.L. and Hewitt, G.M. (2001) Mitochondrial pseudogenes: evolution's misplaced witnesses. *Trends Ecol. Evol.*, **16**, 314–321.
  50. King, M.P. and Attardi, G. (1989) Human cells lacking mtDNA: repopulation with exogenous mitochondria by complementation. *Science*, **246**, 500–503.
  51. Falabella, M., Kolesar, J.E., Wallace, C., de Jesus, D., Sun, L., Taguchi, Y.V., Wang, C., Wang, T., Xiang, I.M., Alder, J.K. *et al.* (2019) G-quadruplex dynamics contribute to regulation of mitochondrial gene expression. *Sci. Rep.*, **9**, 5605.
  52. Lujan, S.A., Longley, M.J., Humble, M.H., Lavender, C.A., Burkholder, A., Blakely, E.L., Alston, C.L., Gorman, G.S., Turnbull, D.M., McFarland, R. *et al.* (2020) Ultrasensitive deletion detection links mitochondrial DNA replication, disease, and aging. *Genome Biol.*, **21**, 248.
  53. Pohjoismaki, J.L.O., Forslund, J.M.E., Goffart, S., Torregrosa-Munumer, R. and Wanrooij, S. (2018) Known unknowns of mammalian mitochondrial DNA maintenance. *Bioessays*, **40**, e1800102.
  54. Lim, S.E. and Copeland, W.C. (2001) Differential incorporation and removal of antiviral deoxynucleotides by human DNA polymerase gamma. *J. Biol. Chem.*, **276**, 23616–23623.
  55. Tyynismaa, H., Sembongi, H., Bokori-Brown, M., Granycome, C., Ashley, N., Poulton, J., Jalanko, A., Spelbrink, J.N., Holt, I.J. and Suomalainen, A. (2004) Twinkle helicase is essential for mtDNA maintenance and regulates mtDNA copy number. *Hum. Mol. Genet.*, **13**, 3219–3227.
  56. Ylikallio, E., Tyynismaa, H., Tsutsui, H., Ide, T. and Suomalainen, A. (2010) High mitochondrial DNA copy number has detrimental effects in mice. *Hum. Mol. Genet.*, **19**, 2695–2705.
  57. Song, J., Herrmann, J.M. and Becker, T. (2021) Quality control of the mitochondrial proteome. *Nat. Rev. Mol. Cell Biol.*, **22**, 54–70.
  58. Tanaka, M., Borgeld, H.J., Zhang, J., Muramatsu, S., Gong, J.S., Yoneda, M., Maruyama, W., Naoi, M., Ibi, T., Sahashi, K. *et al.* (2002) Gene therapy for mitochondrial disease by delivering restriction endonuclease SmaI into mitochondria. *J. Biomed. Sci.*, **9**, 534–541.
  59. Bayona-Bafaluy, M.P., Blits, B., Battersby, B.J., Shoubridge, E.A. and Moraes, C.T. (2005) Rapid directional shift of mitochondrial DNA heteroplasmy in animal tissues by a mitochondrially targeted restriction endonuclease. *Proc. Natl. Acad. Sci. U.S.A.*, **102**, 14392–14397.
  60. Bacman, S.R., Williams, S.L., Pinto, M., Peralta, S. and Moraes, C.T. (2013) Specific elimination of mutant mitochondrial genomes in patient-derived cells by mitoTALENs. *Nat. Med.*, **19**, 1111–1113.
  61. Gammage, P.A., Rorbach, J., Vincent, A.I., Rebar, E.J. and Minczuk, M. (2014) Mitochondrially targeted ZFNs for selective degradation of pathogenic mitochondrial genomes bearing large-scale deletions or point mutations. *EMBO Mol. Med.*, **6**, 458–466.
  62. Bedrat, A., Lacroix, L. and Mergny, J.L. (2016) Re-evaluation of G-quadruplex propensity with G4Hunter. *Nucleic Acids Res.*, **44**, 1746–1759.
  63. Falabella, M., Fernandez, R.J., Johnson, F.B. and Kaufman, B.A. (2019) Potential roles for G-quadruplexes in mitochondria. *Curr. Med. Chem.*, **26**, 2918–2932.
  64. Wanrooij, S., Luoma, P., van Goethem, G., van Broeckhoven, C., Suomalainen, A. and Spelbrink, J.N. (2004) Twinkle and POLG defects enhance age-dependent accumulation of mutations in the control region of mtDNA. *Nucleic Acids Res.*, **32**, 3053–3064.
  65. Krishnan, K.J., Reeve, A.K., Samuels, D.C., Chinnery, P.F., Blackwood, J.K., Taylor, R.W., Wanrooij, S., Spelbrink, J.N., Lightowers, R.N. and Turnbull, D.M. (2008) What causes mitochondrial DNA deletions in human cells? *Nat. Genet.*, **40**, 275–279.
  66. Goffart, S., Cooper, H.M., Tyynismaa, H., Wanrooij, S., Suomalainen, A. and Spelbrink, J.N. (2009) Twinkle mutations associated with autosomal dominant progressive external ophthalmoplegia lead to impaired helicase function and in vivo mtDNA replication stalling. *Hum. Mol. Genet.*, **18**, 328–340.
  67. Pohjoismaki, J.L., Goffart, S. and Spelbrink, J.N. (2011) Replication stalling by catalytically impaired Twinkle induces mitochondrial DNA rearrangements in cultured cells. *Mitochondrion*, **11**, 630–634.
  68. Persson, O., Muthukumar, Y., Basu, S., Jenninger, L., Uhler, J.P., Berglund, A.K., McFarland, R., Taylor, R.W., Gustafsson, C.M., Larsson, E. *et al.* (2019) Copy-choice recombination during mitochondrial L-strand synthesis causes DNA deletions. *Nat. Commun.*, **10**, 759.